Differential Fractionation of Rhyolites During the Course of Crustal Extension, Western Afar (Ethiopian Rift)

Dereje Ayalew, Raphaël Pik, Nicolas Bellahsen, Lyderic France, Gezahegn Yirgu

AGU100 ADVANCING EARTH AND SPACE SCIENCE

Geochemistry, Geophysics, Geosystems

RESEARCH ARTICLE
10.1029/2018GC007446

Special Section:
Magmatic and volcanic processes in continental rifts

Differential Fractionation of Rhyolites During the Course of Crustal Extension, Western Afar (Ethiopian Rift)

Dereje Ayalew[1], Raphaël Pik[2], Nicolas Bellahsen[3], Lydéric France[2], and Gezahegn Yirgu[1]

[1]School of Earth Sciences, Addis Ababa University, Addis Ababa, Ethiopia, [2]CRPG, UMR 7358 CNRS-Université de Lorraine, 15 rue ND des pauvres, BP20, Vandoeuvre-lès-Nancy Cedex, France, [3]Sorbonne Université, CNRS, Institut des Sciences de la Terre Paris, ISTeP UMR 7193, Paris, France

Key Points:
- The origin of rhyolite over the last 30 Ma has been addressed
- An attempt was made to understand the evolution of crustal contamination through time
- The relations between rhyolite genesis and rifting have been constrained

Correspondence to:
D. Ayalew,
dereayal@geol.aau.edu.et

Citation:
Ayalew, D., Pik, R., Bellahsen, N., France, L., & Yirgu, G. (2019). Differential fractionation of rhyolites during the course of crustal extension, Western Afar (Ethiopian rift). *Geochemistry, Geophysics, Geosystems*, *20*, 571–593. https://doi.org/10.1029/2018GC007446

Received 8 MAR 2018
Accepted 24 NOV 2018
Accepted article online 28 NOV 2018
Published online 1 FEB 2019

Abstract We report field observation, age, chemical (major and trace elements), and isotope (Sr-Nd-Pb) data for felsic volcanic rocks from Central Afar and adjacent western margin. Investigated volcanic rocks are dominantly rhyolites with minor trachytes, and they are geochemically similar. Their ages range from ~30 Ma (prerift stage), ~20 Ma (early synrift), ~8–4 Ma (main thinning event) to ~2.5–0.1 Ma (late synrift/continental breakup), representing the entire volcanic-tectonic events that occurred episodically. Major element variations are consistent with fractionation of gabbroic cumulates. Trace element and isotope data preclude an origin by crustal anatexis; the rhyolites are rather genetically linked to the associated basalts and variously contaminated by the crust during differentiation of magmas. Chemical and isotopic data of the rhyolites support an origin by open system differentiation at deep crustal levels (hot wall rock and high r = rate of assimilation/rate of crystallization) and shallow crustal levels (cold wall rock and low r) with a change in the composition of the assimilated material from lower crustal to upper crustal type. Assimilation appears to decrease in recent times with Quaternary rhyolites, emplaced nearby the active magmatic segments in Afar, which exhibit the isotopic compositions closest to original mantle signature. This is compatible with a crust below the active magmatic segments resulting from important addition of juvenile basic magmas. Such results and interpretations provide actual constrains to suggest that the present-day stage is probably very close to continental breakup, which will be achieved once the continental crust will be entirely replaced by new magmatic crust.

1. Introduction

Rhyolites are commonly found in continental rift zones, though their abundances vary obviously from province to province. The abundance of rhyolites is thought to be related to the supply rate of basaltic magma (e.g., Geist et al., 1995; Hutchison et al., 2018; Mahoney et al., 2008); when the input of basaltic magma is high, the system is swamped by basaltic components, whereas when the supply rate of basaltic magma declines or stops, more silicic melts dominate the system. The amount of rhyolite may also be a function of lithospheric extension (e.g., Hutchison et al., 2018; Storey et al., 1995); rhyolites are found at early stage of extension, while basalts are abundant at advanced stage of rifting.

The generation of rhyolites, with SiO_2 contents in excess of 70 wt.%, remains a matter of debated issue. Combination of three end-member mechanisms is commonly invoked to explain such magmas: (1) anatectic melting of crust (e.g., Bohrson & Reid, 1997; Cameron et al., 1996; Pichavant et al., 1988; Riley et al., 2001), (2) remelting of solidified basalt or its derivative intruded within or underplated to the crust during the same volcanic episode (e.g., France et al., 2010, 2014; Garland et al., 1995; Miller & Harris, 2007), and (3) fractional crystallization of a more mafic magma with or without crustal contamination (e.g., France et al., 2016; Hutchison et al., 2018; Macdonald, 2012; Medlin et al., 2014; Natali et al., 2011; Rooney et al., 2012; Thorarinsson et al., 2012). Modeling indicates that evolved melts can be generated simultaneously from both basalt crystallization and crustal partial melting (Annen et al., 2006; Annen & Sparks, 2002). Whether an origin by fractional crystallization or by partial melting for the formation of the rhyolites largely depends on the distance of the rhyolite to the rifted zone (e.g., Selbekk & Trønnes, 2007); partial melting is an important process in the formation of rhyolites erupted near the rift zones, whereas fractional crystallization prevails for rhyolites erupted far from the rift zones. There is yet little consensus on any of these models.

Ethiopia has been the site of extensive bimodal basalt-rhyolite volcanism since 45 Ma (Ebinger et al., 1993; George et al., 1998). The rhyolites are spatially associated with basalts over the entire eruptive period

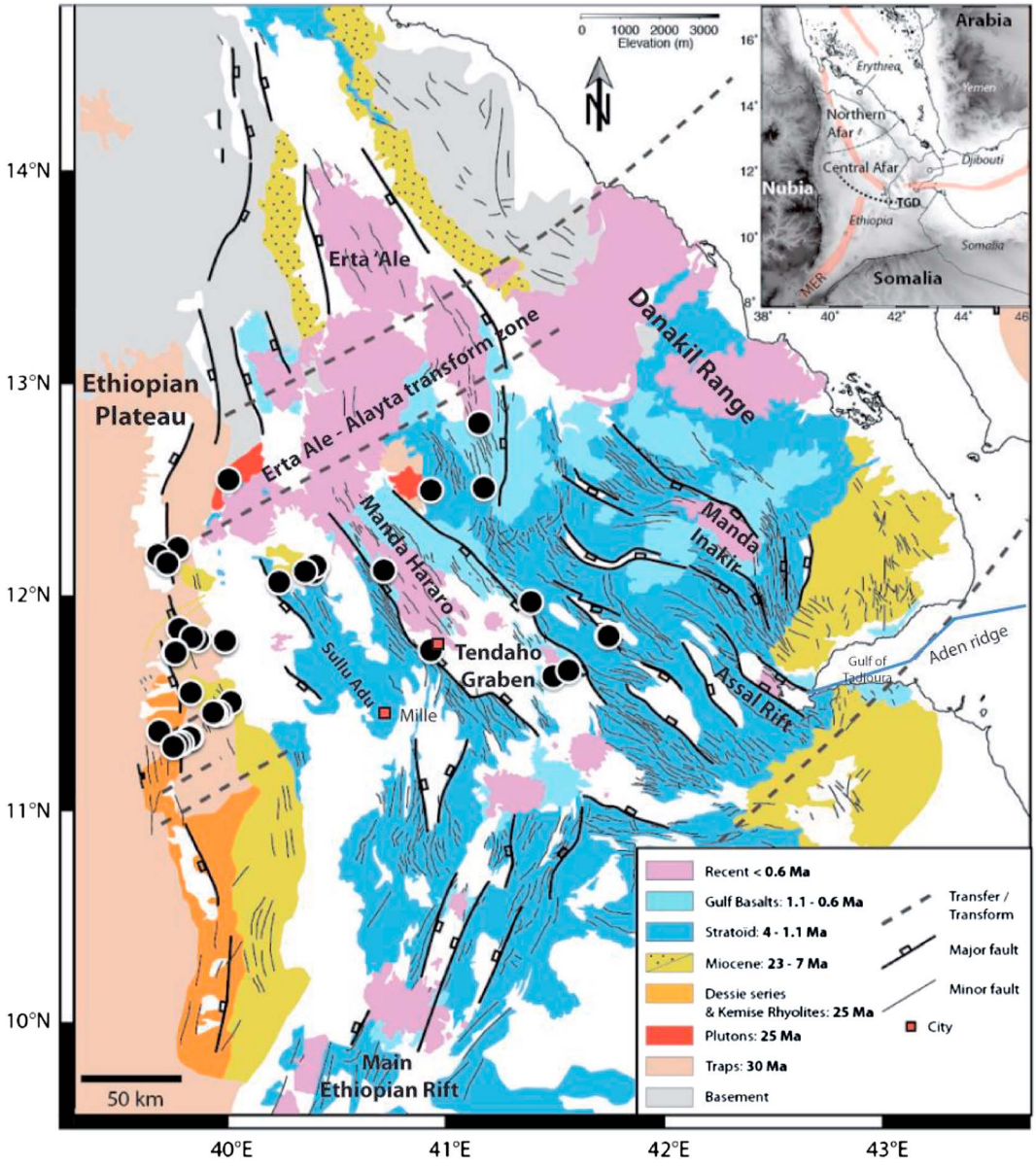

Figure 1. Geological map of the Afar Depression (after Stab et al., 2016), showing the distributions of the investigated samples (filled circles). Inset shows the Afro-Arabian triple rift junction.

(Ayalew et al., 2006). Understanding the process that leads to the formation of rhyolites in bimodal system is a major goal of studies of continental magmatism as it provides valuable information on the interaction between mantle-derived melts and the crust. In this study, we report field observation, age, chemical (major and trace elements), and isotope (Sr-Nd-Pb) data for felsic volcanic rocks emplaced over the entire magmatic episodes ranging in age from ~30 Ma (prerift stage), ~20 Ma (early synrift), ~8–4 Ma (main thinning event) to ~2.5–0.1 Ma (late synrift/continental breakup), from the Ethiopian Plateau down to the active Central Afar volcanic segment (Manda Hararo rift segment; Figure 1). Details of field relations of the investigated samples are reported in Table 1. We use the newly established volcanic-tectonic history of the Central Afar segment (Stab et al., 2016) to examine the geochemical evolution with time of felsic volcanics during the course of rifting as it has progressed to breakup processes expressed in the Afar Depression. Our findings support the new structural (Stab et al., 2016) result of the Western Afar segment.

Table 1
Summary of the Geological Features of the Studied Samples

Sample	Lat.	Long.	Rock type	Age (Ma)	Age justification	Location
Quaternary Afar rhyolites						
AF13-30	12.4789	41.1601	Rhyolite	0.52	Same location as Lahitte et al. (2003) sample 75BI	Tat'Ale active segment
AF13-25	12.7665	41.1389	Ryholite	0.10	Field correlation with Lahitte et al. (2003)	Tat'Ale active segment
AF15-17	11.8065	41.7389	Dacite	2.50	Field correlation with Lahitte et al. (2003)	Stratoïde formation
AF15-19	11.8093	41.7402	Rhyolite	2.50	Field correlation with Lahitte et al. (2003)	Stratoïde formation
AF15-11	11.9622	41.3816	Rhyolite	1.32	Same location as Lahitte et al. (2003) sample 75BY1	Stratoïde formation, Serdo rhyolite, eastern Tendaho graben
AF13-340	11.7417	40.9150	Rhyolite	1.30	Field correlation with Lahitte et al. (2003)	Stratoïde formation, western Tendaho graben
AF15-10	11.6253	41.4859	Rhyolite	0.56	Field correlation with Lahitte et al. (2003)	Borawly volcano, near Assaita, southern Tendaho graben
AF15-07A	11.6519	41.5545	Rhyolite	0.50	Field correlation with Lahitte et al. (2003)	East of Assaita, southern Tendaho graben
AF13-337	12.1058	40.6950	Rhyolitic tuff	0.70	Field correlation with Lahitte et al. (2003)	Interbedded in Gulf basalts, west of Manda Hararo active segment
AF13-335	12.1058	40.6950	Rhyolite	0.70	Field correlation with Lahitte et al. (2003)	Interbedded in Gulf basalts, west of Manda Hararo active segment
Late Miocene-Pliocene margin synrift rhyolites (Bokeksa-Arabati section)						
AF12-15	12.0508	40.2039	Rhyolite	4.00	Stab et al. (2016)	Pliocene horizontal synrift lava, west of Sullu Adu
AF13-74	12.0983	40.3261	Andesite	4.00	Field correlation with Lahitte et al. (2003)	Pliocene intermediate lava = top flow?
AF15-40	12.4657	40.9151	Rhyolite	4.00	Field correlation with Lahitte et al. (2003)	Pliocene horizontal synrift lava, NE Tendaho graben, Da'Aal and Affara Dara
AF12-21	11.4630	39.9355	Rhyolite	7.5	Stab et al. (2016)	Boksa-Arabati section in the margin
Arabati-1	11.5085	39.9812	Rhyolite	7.5	Field correlation with this study Chiffra-1 and Stab et al. (2016)	Boksa-Arabati section in the margin
Arabati-2	11.4645	39.9222	Rhyolite	7.5	Field correlation with this study Chiffra-1 and Stab et al. (2016)	Boksa-Arabati section in the margin
Arabati-3	11.4583	39.9060	Rhyolite	7.5	Field correlation with this study Chiffra-1 and Stab et al. (2016)	Boksa-Arabati section in the margin
Galina-1	11.5510	39.7909	Rhyolite	6.3	This study	Boksa-Arabati section in the margin
AF13-97	11.4637	39.9000	Rhyolite	6.3	Field correlation with this study	Boksa-Arabati section in the margin
Early Miocene margin synrift rhyolites (Marginal graben dykes and Afar Finto section)						
Hara-1	11.8385	39.7392	Rhyolite	21.0	Field correlation with this study Woldia-1	Giant marginal rhyolitic dykes near Woldia-Hara
Hara-2	11.7905	39.8232	Rhyolite	22.6	This study	Giant marginal rhyolitic dykes near Woldia-Hara
Hara-3	11.8041	39.7967	Intermediate	17.4	This study	Marginal dykes near Woldia-Hara
Hara-4	11.7396	39.7218	Rhyolite	17.4	Field correlation with this study	Marginal dykes near Woldia-Hara
Hara-5	11.7350	39.7185	Basaltic trachyandesite	17.4	Field correlation with this study	Marginal dykes near Woldia-Hara
Hara-6	11.7310	39.7190	Rhyolite	17.4	Field correlation with this study	Marginal dykes near Woldia-Hara
AF13-89			Rhyolite	22.0	Field correlation with Stab et al. (2016)	Miocene tilted synrift lava, Finto section
AF12-08	12.1252	40.3798	Rhyolite	22.0	Field correlation with Stab et al. (2016)	Miocene tilted synrift lava, Finto section
AF12-09	12.1253	40.3775	Rhyolite	22.0	Field correlation with Stab et al. (2016)	Miocene tilted synrift lava, Finto section
AF13-73	12.0964	40.3623	Trachyandesite	22.0	Field correlation with Stab et al. (2016)	Miocene tilted synrift lava, Finto section
Oligocene prerift trap rhyolites (marginal graben and plateau)						
AF12-04	12.5125	39.9705	Granite	29.0	Field correlation with this study	Limmo granite, bottom of the margin
AF12-10	12.1236	40.3736	Rhyolite	29.7	Stab et al. (2016)	Oligocene tilted basement rhyolite of Finto section
AF13-92R	11.7850	39.9541	Rhyolite	29.0	Field correlation with Stab et al. (2016)	Oligocene tilted basement rhyolite of Allale Sullula, bottom margin
AF13-92	11.7850	39.9541	Trachyandesite	29.0	Field correlation with Stab et al. (2016)	Oligocene tilted basement rhyolite of Allale Sullula, bottom margin
Hayk-1	11.3747	39.6471	Rhyolite	29.0	Field correlation with this study	Marginal graben rhyolites, Hayk section

Table 1 *(continued)*

Sample	Lat.	Long.	Rock type	Age (Ma)	Age justification	Location
Hayk-2	11.3580	39.7867	Rhyolite	29.9	This study	Marginal graben rhyolites, Hayk section
Hayk-3	11.3527	39.7907	Rhyolite	28.5	This study	Marginal graben rhyolites, Hayk section
Hayk-4	11.3521	39.7907	Rhyolite	29.5	This study	Marginal graben rhyolites, Hayk section
Arabati-4	11.3507	39.7899	Rhyolite	29.0	Field correlation with this study	Marginal graben rhyolites, Hayk section
Hayk-5	11.3505	39.7850	Rhyolite	29.0	Field correlation with this study	Marginal graben rhyolites, Hayk section
Arabati-5	11.3255	39.7506	Rhyolite	29.0	Field correlation with this study	Marginal graben rhyolites, Hayk section
Hayk-6	11.3166	39.7331	Rhyolite	30.8	This study	Marginal graben rhyolites, Hayk section
Hayk-7	11.3077	39.7123	Rhyolite	29.3	This study	Marginal graben rhyolites, Hayk section
Kobo-1	12.2037	39.7300	Rhyolite	29.0	Field correlation with this study	Dyke Kobo section
Kobo-3	12.1739	39.6379	Rhyolite	28.7	This study	Granophyre Kobo plain
Kobo-8	12.1351	39.6854	Rhyolite	29.0	Field correlation with this study	Granophyre Kobo plain

2. Geological Background

The magmatic and tectonic events of the region from western marginal graben to active magmatic segment in the Afar Depression have been well documented recently by Doubre et al. (2007), Kogan et al. (2012), Lahitte et al. (2003), McClusky et al. (2010), Medynski et al. (2013, 2015, 2016), and Stab et al. (2016). Volcanism began in the early Oligocene prior to the onset of significant extension, with extrusion of huge volumes of flood basalts and associated rhyolites (Ayalew et al., 2002; Pik et al., 1999; Zanettin & Piccirillo, 1980), forming the so-called spectacular Ethiopian high-plateau between 31 and 29 Ma (Hofmann et al., 1997). The early magmatic episode traditionally referred to as continental flood basalt or traps formation exposed along both sides of the rift escarpments and locally in the Afar Depression (Varet, 1975). Following the end of traps formation, the Dessie formation (mainly basalts) emplaced at 25 Ma (Ukstins et al., 2002). The Dessie formation is locally restricted to the present-day marginal graben and overlies conformably the traps formation. During the Miocene, volcanic activity decreased and occurred in two phases first at 23–22 Ma and second at 8–6 Ma (Stab et al., 2016). The Miocene formations are variably named Chifra series or Finto series and mainly consist of felsic products that are tilted and unconformably overlying the

Table 2
U-Th-Sm)/He Dating of Zircons From Ethiopian Marginal Rhyolites

Sample	Lat.	Long.	Weight (mg)	Length (μm)	Width (μm)	FT mean	^{4}He (mol/g)	^{232}Th (ppm)	^{238}U (ppm)	^{147}Sm (ppm)	Age (Ma)	Corrected age (Ma)	Uncertainty (±Ma)
Late Miocene margin synrift rhyolites (Bokeksa-Arabati section)													
Chiffra #1	11.6043	40.0116	0.0209	304	148	0.86	6.77E−09	94	171	33	6.5	**7.6**	0.5
Chiffra #2			0.0239	321	153	0.86	6.19E−09	89	155	61	6.5	**7.5**	0.5
Galina-1 #1	11.5510	39.7909	0.056	308	155	0.88	1.09E−07	3228	2578	208	6.0	**6.8**	0.4
Galina-1 #2			0.023	265	140	0.87	1.23E−07	1869	4176	156	5.0	**5.7**	0.3
Early Miocene margin synrift rhyolites (Marginal graben dykes and Afar Finto section)													
Hara-2 #1	11.7905	39.8232	0.094	377	222	0.91	4.86E−07	7099	2383	485	22.2	24.3	1.5
Hara-2 #2			0.157	389	226	0.91	3.55E−07	5309	1931	356	20.6	22.6	1.4
Hara-3	11.8041	39.7967	0.086	389	226	0.92	1.68E−08	101	171	78	16.0	17.4	1.0
Woldia-1 #1	11.8784	39.6969	0.048	201	124	0.84	4.38E−08	212	414	73	17.5	20.9	1.3
Woldial-1 #2			0.077	314	139	0.88	3.96E−08	196	370	70	17.6	20.0	1.2
Oligocene prerift trap rhyolites (marginal graben and plateau)													
Kobo3	12.1739	39.6379	0.096	245	183	0.87	9.44E−08	1773	281	117	25.0	28.7	1.7
Hayk-2	11.3580	39.7867	0.02	314	123	0.87	4.45E−08	229	261	317	26.2	29.9	1.8
Hayk-3	11.3527	39.7907	0.028	220	147	0.86	1.53E−07	1415	824	120	24.5	28.5	1.7
Hayk-4	11.3521	39.7907	0.033	243	135	0.86	1.09E−07	1298	491	1459	25.4	29.5	1.8
Hayk-6	11.3166	39.7331	0.095	324	247	0.87	1.35E−07	1352	609	3718	26.9	30.8	1.8
Hayk-7	11.3077	39.7123	0.049	312	151	0.88	8.15E−08	688	425	89	25.7	29.3	1.8

Table 3
Major (wt%) and Trace (ppm) Element Analyses of Felsic Volcanic Rocks From Western Afar Segment

	Oligocene prerift trap rhyolites									
Sample	AF13-337	AF15-17	AF15-19	AF13-335	AF13-25	AF15-10	AF13-340	AF13-30	AF15-11	AF15-07A
Age (Ma)	0.70	2.50	2.50	0.7	0.10	0.56	1.30	0.52	1.32	0.50
Lat.	12.1058	11.8065	11.8093	12.1058	12.7665	11.6253	11.7417	12.4789	11.9622	11.6519
Long.	40.6950	41.7389	41.7402	40.6950	41.1389	41.4859	40.9150	41.1601	41.3816	41.5545
SiO_2	63.51	64.52	66.15	66.66	67.98	70.64	70.72	72.21	73.02	74.82
TiO_2	0.35	1.13	0.57	0.42	0.66	0.23	0.30	0.23	0.23	0.19
Al_2O_3	11.80	12.84	13.74	13.10	12.82	14.34	12.51	12.26	12.75	12.89
Fe_2O_3	3.48	8.88	4.51	4.58	5.60	3.25	4.06	3.36	3.45	1.45
MnO	0.09	0.18	0.11	0.14	0.14	0.10	0.07	0.07	0.08	0.04
MgO	0.51	0.76	0.74	0.30	0.59	0.11	0.23	0.06	0.09	0.18
CaO	3.83	2.53	2.12	2.24	2.23	1.22	0.77	0.99	0.73	1.22
Na_2O	3.77	4.27	3.91	4.06	4.06	4.88	4.13	4.20	4.70	3.67
K_2O	4.09	2.63	3.63	3.98	3.59	3.97	4.34	4.35	4.03	4.25
P_2O_5	LD	0.39	LD	LD	0.17	LD	LD	LD	LD	LD
Total	91.42	98.13	95.46	95.47	97.85	98.74	97.13	97.72	99.09	98.71
LOI	8.18	1.45	3.50	4.76	2.07	1.30	1.72	1.46	0.86	1.46
Be	4.4	3.4	3.7	4.7	4.3	4.6	6.2	4.2	6.4	3.1
V	12.6	11.0	1.8	10.0	15.7	4.5	2.2	5.7	3.7	3.4
Zn	122	168	113	141	143	140	158	120	191	33
Ga	22.2	27.3	24.3	24.6	26.9	29.9	27.5	26.2	31.7	16.8
Ge	1.8	2.2	1.5	2.1	1.9	2.2	2.1	1.7	2.4	1.3
Rb	80	65	72	84	73	82	104	99	87	109
Sr	207	240	158	144	167	122	85	98	116	98
Y	78	82	84	89	94	90	99	79	106	27
Zr	586	669	728	750	806	562	855	678	613	178
Nb	66	71	65	86	85	97	111	72	121	23
Sn	7.0	6.5	7.3	8.2	6.2	7.8	9.8	5.3	8.9	3.8
Cs	0.9	1.4	4.0	1.0	1.0	1.2	0.8	1.5	0.5	1.3
Ba	695	531	534	692	615	892	827	989	827	694
La	70	69	69	77	84	107	100	80	106	52
Ce	148	141	140	162	181	216	205	166	218	89
Pr	17.33	17.62	16.97	19.58	22.03	25.23	24.80	20.11	27.84	8.95
Nd	67	73	67	76	86	95	94	78	108	29
Sm	14.04	16.66	15.06	16.12	18.56	18.84	19.44	16.38	22.98	5.17
Eu	2.66	4.63	3.56	3.30	4.26	3.76	3.63	3.18	5.14	1.07
Gd	12.85	15.65	13.93	14.64	16.80	16.32	17.24	14.63	20.35	4.37
Tb	2.17	2.60	2.40	2.50	2.77	2.71	2.94	2.41	3.40	0.70
Dy	14.04	15.94	15.06	16.17	16.57	16.85	18.42	14.60	20.64	4.52
Ho	3.02	3.25	3.15	3.48	3.29	3.49	3.87	2.82	4.20	0.96
Er	8.44	8.55	8.58	9.77	9.17	9.50	10.56	7.93	11.07	2.79
Tm	1.22	1.18	1.21	1.44	1.38	1.36	1.51	1.23	1.54	0.42
Yb	8.31	7.93	8.38	9.80	8.95	9.45	10.34	8.08	10.41	3.02
Lu	1.24	1.18	1.27	1.48	1.34	1.42	1.57	1.19	1.54	0.47
Hf	16.2	16.4	18.3	19.9	18.4	15.7	21.5	16.2	19.0	5.3
Ta	5.2	5.5	5.3	6.5	6.4	7.6	8.7	5.4	9.4	2.9
Pb	9.9	6.9	7.4	10.2	10.9	10.2	12.0	10.1	9.8	9.9
Th	10.9	9.6	12.8	12.0	11.2	15.1	17.4	12.5	15.1	16.9
U	2.9	2.7	3.7	3.1	2.9	3.5	4.2	3.0	3.0	4.1

	Late Miocene-Pliocene margin synrift rhyolites (Bokeksa-Arabati section)						
Sample	AF13-74	Arabati-2	AF15-40	AF12-15	Arabati-3	AF12-21	Galina-1
Age (Ma)	4.00	7.5	4.00	4.00	7.5	7.50	6.3
Lat.	12.0983	11.4645	12.4657	12.0508	11.4583	11.4630	11.5510
Long.	40.3261	39.9222	40.9151	40.2039	39.9060	39.9355	39.7909
SiO_2	59.33	67.78	71.12	74.49	75.80	76.78	77.08
TiO_2	1.79	0.50	0.38	0.18	0.20	0.14	0.06
Al_2O_3	13.50	13.42	12.73	12.21	11.42	11.90	11.34
Fe_2O_3	8.91	3.90	3.93	1.80	1.87	1.36	1.39

Table 3 *(continued)*

	Late Miocene-Pliocene margin synrift rhyolites (Bokeksa-Arabati section)						
Sample	AF13-74	Arabati-2	AF15-40	AF12-15	Arabati-3	AF12-21	Galina-1
Age (Ma)	4.00	7.5	4.00	4.00	7.5	7.50	6.3
Lat.	12.0983	11.4645	12.4657	12.0508	11.4583	11.4630	11.5510
Long.	40.3261	39.9222	40.9151	40.2039	39.9060	39.9355	39.7909
MnO	0.14	0.04	0.11	0.02	0.01	0.00	0.01
MgO	1.75	0.23	0.24	0.06	0.03	0.05	0.12
CaO	4.94	1.55	0.86	0.79	0.19	0.09	0.16
Na_2O	4.12	2.93	4.58	3.28	3.81	3.94	2.91
K_2O	1.65	5.17	4.07	5.18	4.77	4.90	4.29
P_2O_5	0.57	0.10	LD	0.13	LD	LD	LD
Total	96.70	95.63	98.02	98.14	98.08	99.16	97.36
LOI	2.56	4.26	1.63	1.17	0.93	0.30	1.46
Be	2.5	4.7	3.6	3.8	4.0	4.0	9.3
V	126	15.3	18.6	5.9	0.8	4.8	5.5
Zn	140	68	119	69	127	75	110
Ga	25.8	21.4	24.8	24.0	31.7	28.1	28.0
Ge	1.5	1.6	2.0	1.4	1.8	1.6	2.4
Rb	145	123	82	143	142	182	311
Sr	450	97	107	27	5.9	4.8	7.6
Y	44	92	68	57	114	82	30
Zr	378	489	570	272	834	418	176
Nb	31	15	76	36	48	29	46
Sn	3.8	7.3	6.9	7.6	14.0	9.9	15.6
Cs	1.9	2.6	0.5	1.1	1.0	2.7	2.4
Ba	618	865	851	274	13	14	16
La	44	55	77	59	11	79	15
Ce	95	97	155	115	35	146	58
Pr	12.4	13.6	19.1	14.1	3.4	20.6	3.0
Nd	52.5	53.9	73.6	52.7	15.0	80.2	9.9
Sm	11.9	11.7	15.1	10.7	6.0	17.9	2.4
Eu	3.25	1.65	2.96	0.63	0.44	0.42	0.09
Gd	10.39	11.43	13.31	9.48	10.20	15.60	2.33
Tb	1.55	1.92	2.15	1.61	2.34	2.61	0.57
Dy	8.70	12.48	13.28	10.37	18.24	16.25	4.47
Ho	1.56	2.61	2.72	2.22	4.13	3.38	1.10
Er	4.06	7.97	7.36	6.09	13.38	8.98	4.38
Tm	0.57	1.23	1.04	0.92	2.16	1.34	0.95
Yb	3.57	7.87	7.04	6.29	14.86	9.11	8.07
Lu	0.52	1.22	1.04	0.95	2.20	1.30	1.31
Hf	9.0	11.9	16.8	9.2	22.9	13.8	9.6
Ta	2.5	1.2	5.8	2.9	3.9	2.3	5.4
Pb	13.6	20.6	11.0	17.0	9.5	17.4	57.0
Th	9.3	13.8	11.8	15.2	19.8	18.2	30.7
U	4.7	4.6	2.8	4.3	4.7	5.7	11.9

	Early Miocene margin synrift rhyolites (Marginal graben dykes and Afar Finto section)									
Sample	Hara-5	AF13-73	Hara-3	AF12-09	Hara-2	Hara-6	Hara-4	Hara-1	AF12-08	AF13-89
Age (Ma)	17.4	22.00	17.4	22.00	22.6	17.4	17.4	21	22.00	22.00
Lat.	11.7350	12.0964	11.8041	12.1253	11.7905	11.7310	11.7396	11.8385	12.1252	
Long.	39.7185	40.3623	39.7967	40.3775	39.8232	39.7190	39.7218	39.7392	40.3798	
SiO_2	51.47	57.51	62.97	67.30	71.21	72.28	72.87	72.97	74.78	76.60
TiO_2	2.29	1.72	1.60	0.65	0.71	0.63	0.57	0.60	0.48	0.48
Al_2O_3	16.44	12.83	13.01	13.03	13.44	12.51	12.38	12.27	11.68	10.05
Fe_2O_3	9.55	8.54	6.79	3.27	3.39	3.18	2.98	3.26	2.11	2.64
MnO	0.11	0.08	0.17	0.21	0.15	0.12	0.13	0.13	0.02	0.04
MgO	2.80	1.35	2.16	0.51	0.08	0.10	0.14	0.08	0.08	0.06
CaO	6.23	4.80	2.98	0.97	0.13	0.67	0.21	0.11	0.35	0.22
Na_2O	3.72	2.97	4.40	3.58	4.26	3.62	4.03	3.74	4.26	3.13
K_2O	2.36	3.04	3.24	6.24	4.31	5.14	4.53	4.61	4.86	4.55

Table 3 *(continued)*

	Early Miocene margin synrift rhyolites (Marginal graben dykes and Afar Finto section)									
Sample	Hara-5	AF13-73	Hara-3	AF12-09	Hara-2	Hara-6	Hara-4	Hara-1	AF12-08	AF13-89
Age (Ma)	17.4	22.00	17.4	22.00	22.6	17.4	17.4	21	22.00	22.00
Lat.	11.7350	12.0964	11.8041	12.1253	11.7905	11.7310	11.7396	11.8385	12.1252	
Long.	39.7185	40.3623	39.7967	40.3775	39.8232	39.7190	39.7218	39.7392	40.3798	
P_2O_5	0.66	0.43	0.37	0.09	0.09	0.09	0.08	0.07	0.09	0.07
Total	95.64	93.27	97.68	95.84	97.76	98.35	97.92	97.84	98.71	97.82
LOI	3.89	5.49	1.87	3.99	1.32	1.49	1.48	1.11	0.56	0.98
Be	2.5	2.2	3.7	4.4	3.3	3.8	4.0	4.5	5.3	3.8
V	194	159	113	17	22	15	13	14	11	12
Zn	125	113	147	179	166	145	154	150	98	124
Ga	26.9	21.5	28.3	32.1	31.9	31.8	33.5	32.8	34.4	29.4
Ge	1.5	1.2	2.1	2.1	2.2	2.0	2.2	2.5	2.5	2.0
Rb	46	83	60	141	72	84	80	81	126	89
Sr	843	238	324	282	118	77	35	26	26	18
Y	38	36	54	64	61	61	64	67	76	55
Zr	464	320	523	706	448	537	575	616	935	544
Nb	48	25	52	84	56	64	67	72	102	67
Sn	3.7	5.0	4.7	6.6	8.3	6.0	6.4	6.7	8.4	5.7
Cs	0.7	0.4	LD	2.1	0.2	0.4	0.6	0.4	0.4	0.7
Ba	854	582	773	1138	1039	805	742	691	327	515
La	58	39	79	88	126	108	100	112	94	71
Ce	131	84	172	194	207	229	224	243	211	154
Pr	17.02	10.58	21.02	23.66	33.06	27.87	26.28	29.27	25.27	18.97
Nd	70	44	83	94	132	109	102	115	97	75
Sm	13.5	9.9	15.9	18.5	23.3	19.7	19.3	21	20.3	15.7
Eu	3.98	2.78	4.12	5.27	5.98	5.01	4.93	5.19	4.30	3.85
Gd	10.99	8.73	13.10	14.91	17.72	15.38	15.18	16.03	16.69	12.80
Tb	1.53	1.30	1.92	2.22	2.54	2.30	2.30	2.47	2.63	1.91
Dy	8.01	7.48	10.83	12.92	13.31	12.44	13.04	13.62	15.54	11.19
Ho	1.39	1.43	1.97	2.49	2.29	2.22	2.34	2.43	3.02	2.11
Er	3.58	3.50	5.37	6.27	5.77	5.88	6.40	6.42	7.60	5.34
Tm	0.50	0.47	0.76	0.85	0.80	0.83	0.89	0.91	1.06	0.72
Yb	3.15	3.04	4.84	5.60	5.01	5.36	5.81	5.84	6.83	4.72
Lu	0.45	0.44	0.74	0.82	0.73	0.79	0.85	0.85	0.98	0.68
Hf	10.8	7.9	11.8	16.3	10.8	12.8	13.6	14.4	22.0	12.7
Ta	3.6	2.0	3.9	6.5	4.1	4.7	5.1	5.4	7.9	4.9
Pb	7.9	9.9	10.0	15.1	11.8	11.1	13.5	13.7	11.8	9.1
Th	7.9	7.6	9.2	12.4	10.1	11.4	12.5	12.9	16.4	9.7
U	2.6	3.1	3.0	3.8	3.3	2.9	3.4	3.1	2.7	3.8

	Oligocene prerift trap rhyolites (marginal graben and plateau)									
Sample	AF13-92	Kobo-3	Hayk-6	Arab-4	Hayk-3	Kobo-1	Hayk-4	AF13-92R	Arab-5	Kobo-8
Age (Ma)	29	28.7	30.8	29	28.5	29	29.5	29.00	29	29
Lat.	11.7850	12.1739	11.3166	11.3507	11.3527	12.2037	11.3521	11.7850	11.3255	12.1351
Long.	39.9541	39.6379	39.7331	39.7899	39.7907	39.7300	39.7907	39.9541	39.7506	39.6854
SiO_2	58.41	68.98	69.41	70.42	71.50	72.01	72.32	73.53	73.94	74.30
TiO_2	2.01	0.65	0.61	0.71	0.63	0.63	0.54	0.14	0.50	0.49
Al_2O_3	14.88	14.08	11.75	13.67	13.69	11.60	12.76	11.43	12.84	9.44
Fe_2O_3	8.64	3.23	3.29	3.40	3.11	4.78	3.38	1.99	1.80	5.32
MnO	0.10	0.17	0.10	0.23	0.07	0.24	0.15	0.02	0.04	0.21
MgO	1.06	0.27	0.33	0.20	0.19	0.26	0.14	0.04	LD	0.21
CaO	4.08	0.28	1.73	0.19	0.18	0.27	0.13	0.31	0.06	0.30
Na_2O	4.30	5.74	4.32	4.92	3.53	4.64	1.84	2.22	4.59	3.49
K_2O	2.47	4.82	4.44	4.34	4.68	4.65	4.67	6.14	4.45	4.56
P_2O_5	0.62	0.07	0.13	0.08	0.06	0.09	LD	LD	LD	LD
Total	96.57	98.30	96.09	98.15	97.63	99.15	95.92	95.81	98.22	98.31
LOI	2.55	0.74	2.53	1.97	3.22	1.65	3.79	3.36	0.83	1.33
Be	2.0	8.1	6.3	6.6	7.9	6.7	6.2	5.3	6.5	11.4
V	151	12.4	15.9	18.5	17.0	18.2	16.7	1.7	8.6	12.9

Table 3 *(continued)*

	Oligocene prerift trap rhyolites (marginal graben and plateau)									
Sample	AF13-92	Kobo-3	Hayk-6	Arab-4	Hayk-3	Kobo-1	Hayk-4	AF13-92R	Arab-5	Kobo-8
Age (Ma)	29	28.7	30.8	29	28.5	29	29.5	29.00	29	29
Lat.	11.7850	12.1739	11.3166	11.3507	11.3527	12.2037	11.3521	11.7850	11.3255	12.1351
Long.	39.9541	39.6379	39.7331	39.7899	39.7907	39.7300	39.7907	39.9541	39.7506	39.6854
Zn	102	160	170	168	129	203	143	116	82	273
Ga	19.4	36.4	32.6	32.1	36.9	36.7	32.5	27.6	31.8	33.3
Ge	1.4	2.6	2.6	2.7	3.1	2.5	3.1	1.8	2.6	3.3
Rb	46	104	113	97	110	96	100	211	97	161
Sr	888	14	54	150	26	34	20	5.3	45.8	10.4
Y	34.9	63.2	71.8	65.8	88.5	55.0	94.8	100.4	61.6	131.5
Zr	451	936	824	715	975	765	967	424	759	1237
Nb	44.0	108.5	95.6	83.0	108.2	84.0	125.0	29.7	75.0	150.4
Sn	2.8	9.0	9.4	6.9	11.2	6.7	11.6	10.8	7.7	16.9
Cs	0.5	1.3	0.9	1.1	0.9	0.6	0.4	3.9	0.5	1.1
Ba	856	267	482	1043	324	668	402	19	792	200
La	53.19	98.33	101.20	96.42	95.78	101.30	85.23	68.98	91.87	92.57
Ce	119	216	222	186	217	203	202	143	190	267
Pr	15.58	25.37	26.49	24.78	26.50	24.49	25.51	17.46	23.62	28.40
Nd	63.85	95.62	101.50	98.88	101.80	91.87	97.00	68.04	89.27	111.60
Sm	12.64	17.56	20.17	18.66	21.03	17.51	21.09	15.61	17.05	26.60
Eu	3.66	3.41	4.45	5.25	4.52	4.75	4.59	0.28	3.78	6.59
Gd	9.91	13.71	16.31	15.11	17.88	13.80	18.09	15.04	13.27	25.15
Tb	1.38	2.13	2.56	2.27	2.90	2.13	2.99	2.57	2.08	4.09
Dy	7.17	11.97	14.29	12.44	16.99	11.49	17.58	17.02	11.95	23.71
Ho	1.26	2.20	2.58	2.28	3.12	2.04	3.30	3.73	2.19	4.54
Er	3.24	6.16	7.00	6.02	8.60	5.34	9.23	10.35	6.31	12.52
Tm	0.44	0.89	0.99	0.87	1.27	0.72	1.32	1.53	0.94	1.76
Yb	2.76	5.83	6.47	5.54	8.15	4.54	8.62	10.52	6.37	11.31
Lu	0.40	0.86	0.96	0.81	1.21	0.67	1.29	1.52	0.94	1.68
Hf	9.8	23.7	20.5	16.0	24.9	15.2	24.5	13.9	17.5	32.3
Ta	3.3	8.7	7.6	6.4	9.0	6.5	9.3	2.3	5.9	11.3
Pb	5.7	17.8	18.2	15.6	18.6	11.8	21.2	25.3	15.8	26.9
Th	5.9	19.9	18.7	15.3	22.4	12.3	22.2	18.4	15.0	29.8
U	1.8	6.0	5.7	4.3	6.0	2.5	6.8	5.8	4.4	6.6

	Oligocene prerift trap rhyolites					
Sample	Hayk-7	AF12-04	Hayk-1	AF12-10	Hayk-2	Hayk-5
Age (Ma)	29.3	29.00	29	29.70	29.9	29
Lat.	11.3077	12.5125	11.3747	12.1236	11.3580	11.3505
Long.	39.7123	39.9705	39.6471	40.3736	39.7867	39.7850
SiO_2	74.35	74.46	74.70	75.29	80.55	81.70
TiO_2	0.55	0.33	0.48	0.41	0.47	0.48
Al_2O_3	11.11	12.56	11.64	11.66	8.07	7.91
Fe_2O_3	2.77	2.62	2.91	2.53	2.26	2.57
MnO	0.05	0.11	0.12	0.05	0.08	0.09
MgO	0.08	0.19	0.18	0.11	0.04	0.08
CaO	0.32	0.24	0.18	0.35	0.44	0.24
Na_2O	3.87	4.19	4.60	4.10	2.53	2.52
K_2O	4.64	4.29	4.60	4.74	3.41	3.23
P_2O_5	0.15	LD	0.07	0.05	0.16	0.16
Total	97.88	99.00	99.48	99.29	98.02	98.97
LOI	1.49	1.21	0.64	0.93	1.34	1.33
Be	6.3	4.7	7.0	3.9	4.1	4.5
V	27.0	4.1	9.8	8.8	8.5	9.6
Zn	120	140	168	124	82	81
Ga	28.9	30.6	31.2	30.5	20.4	20.5
Ge	2.0	1.7	3.0	2.1	3.5	3.0
Rb	105	108	116	118	62	62
Sr	38	68	54	15	42	44

Table 3 *(continued)*

	Oligocene prerift trap rhyolites					
Sample	Hayk-7	AF12-04	Hayk-1	AF12-10	Hayk-2	Hayk-5
Age (Ma)	29.3	29.00	29	29.70	29.9	29
Lat.	11.3077	12.5125	11.3747	12.1236	11.3580	11.3505
Long.	39.7123	39.9705	39.6471	40.3736	39.7867	39.7850
Y	68.4	75.8	91.8	67.2	44.7	48.0
Zr	774	609	862	957	519	555
Nb	85	83	100	87	53	54
Sn	8.1	7.7	7.6	7.9	4.5	5.1
Cs	0.7	1.7	1.2	0.3	0.3	0.3
Ba	404	715	384	278	540	486
La	87.15	82.45	84.64	117.60	63.58	70.56
Ce	189	207	183	246	134	138
Pr	23.22	22.46	23.57	28.09	16.31	17.87
Nd	89	87	92	104	63	69
Sm	18.56	18.03	19.42	19.66	12.26	13.14
Eu	4.09	3.30	4.41	3.58	3.03	3.22
Gd	15.35	15.10	17.14	15.45	9.88	10.73
Tb	2.41	2.41	2.73	2.34	1.53	1.63
Dy	13.46	14.98	16.24	13.74	8.56	9.15
Ho	2.47	3.02	3.07	2.64	1.55	1.67
Er	6.75	8.04	8.55	6.72	4.24	4.56
Tm	0.96	1.17	1.28	0.94	0.61	0.66
Yb	6.26	7.86	8.21	6.22	3.97	4.18
Lu	0.94	1.16	1.23	0.92	0.60	0.64
Hf	19.4	16.0	21.9	21.8	11.7	12.4
Ta	6.9	6.5	8.0	6.5	4.0	4.2
Pb	14.4	14.1	15.0	18.0	9.4	8.1
Th	17.2	13.6	19.7	15.7	10.5	11.3
U	5.8	4.0	7.0	1.7	4.0	3.9

Note. Samples are arranged with increasing order of SiO_2 contents within each suite. LD, below detection limit; LOI, loss on ignition. Total iron as Fe_2O_3. Major elements were determined by inductively coupled plasma atomic emission spectroscopy while trace elements by inductively coupled plasma-mass spectrometry at CRPG, Nancy (France).

traps or Dessie formations. During the Pliocene, a second pulse of flood basalts with some acidic eruptives occurred at ~4 Ma, with a major emission around 2 Ma termed as Stratoïde formation (Varet, 1975). The Stratoïde formation is covered by the Gulf basalts extruded between approximately 1.1 and 0.6 Ma along with some silicic centers (Kidane et al., 2003). Present-day magmatism is restricted along the rift axis (Medynski et al., 2013, 2015, 2016) and manifested as dyke injection in the crust with few eruptions (Wright et al., 2006).

Rifting is thought to begin in southern Red Sea between 26 and 20 Ma (Baker et al., 1996; Ukstins et al., 2002), in Afar after 29 Ma (Ukstins et al., 2002; Wolfenden et al., 2005), around 34 Ma in the whole Gulf of Aden (Leroy et al., 2012; Pik et al., 2013, and references therein), and at approximately 18–20 Ma in the Main Ethiopian Rift (Pik et al., 2008; Woldegabriel et al., 1990).

The thickness of the crust beneath Ethiopia is well constrained by receiver function studies (Dugda et al., 2005; Hammond et al., 2011; Reed et al., 2014) and varies from 40 to 45 km underneath the western plateau to ~35 km under the southeastern plateau. The crust in the Afar Depression thins from 25 km in Central Afar to ~16 km in the North (Northern Afar, Erta Ale). The receiver function studies further indicate the presence of significant amounts of melt throughout a large part of the crust. In Central Afar, a magmatic wide rift (including the present-day marginal graben) was most likely active after the traps emplacement during an early rifting stage. At the end of the Miocene, the rifting localized at depth along a midcrustal detachment, which subsequently controlled the Stratoïde emplacement (Stab et al., 2016). The divergence then localized in magmatic segments (Ebinger & Casey, 2001; Hayward & Ebinger, 1996; Stab et al., 2016).

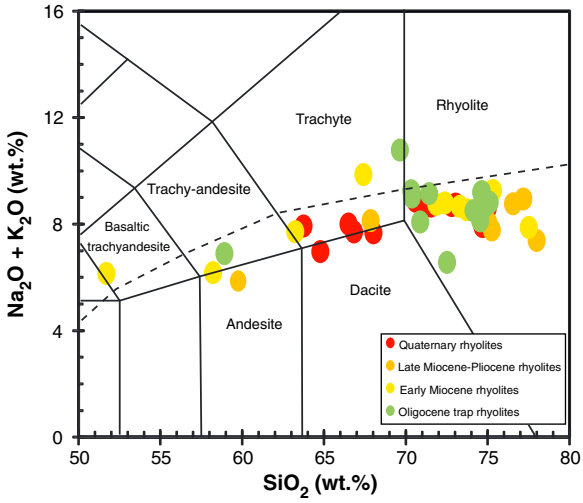

Figure 2. Total alkali-silica classification diagram (TAS, LeBas et al., 1986) of the volcanic rocks from Western Afar marginal graben, indicating more abundant rhyolites. Alkaline-subalkaline dividing boundary (dashed line) is from Irvine and Baragar (1971).

3. Analytical Procedures

The Sr-Nd-Pb isotope separations were done using the same aliquot of the sample. Between 100 and 200 mg of fine-grained powder (particle size lower than 80 μm) were digested into 15-ml teflon beakers using a mixture of concentrated ultrapure acid (HNO_3 and HF). The mixture was heated at 115 °C for 24–48 hr before adding concentrated ultrapure HCl and heated till complete digestion (at least 24 hr). Before further purification each sample was splitted into two parts for Pb separation from one hand and for Sr-Nd separation on a second hand.

Lead was separated from the matrix using HBr-HCl and AG1X8 (anionic chromatographic) resin according to a similar method previously published by Manhès et al. (1980). The samples dissolved in 1 ml 0.8 M HBr were loaded onto the resin, the matrix were washed with 2 ml of 0.8 M HBr, and then the Pb was recovered from the resin using 2 ml of 6 M HCl. Once dried the samples were dissolved in 0.3 M HNO_3 and ready for measurements. Isotopic analyses were done using a MC-ICPMS Neptune+ (Thermo Scientific). Mass bias was corrected using Tl (NIST 997) and Pb (NIST 981) international standard and values previously published by Thirlwall (2002). More details are available elsewhere (White et al., 2000).

To separate Sr and Nd from the matrix, the digested samples were diluted using 2 ml of 2M HNO_3 and done according to the analytical protocol published by Pin and Zalduegui (1997) using Sr Spec and TRU Spec resin combination. To further separate Nd from Sm and other REE (rare earth elements), an additional stage of purification was done using Ln Spec resin as suggested previously by Pin and Zalduegui (1997).

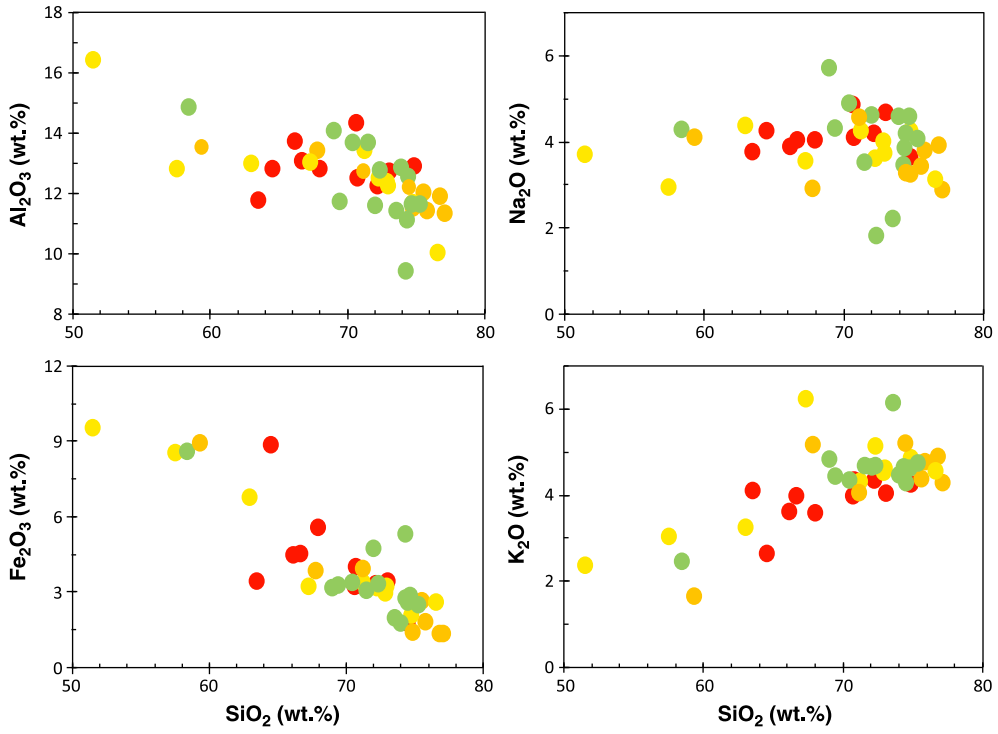

Figure 3. Harker variation diagrams for marginal rhyolites from Western Afar, showing fractionation of Fe- and Al-bearing minerals. Symbols as Figure 2.

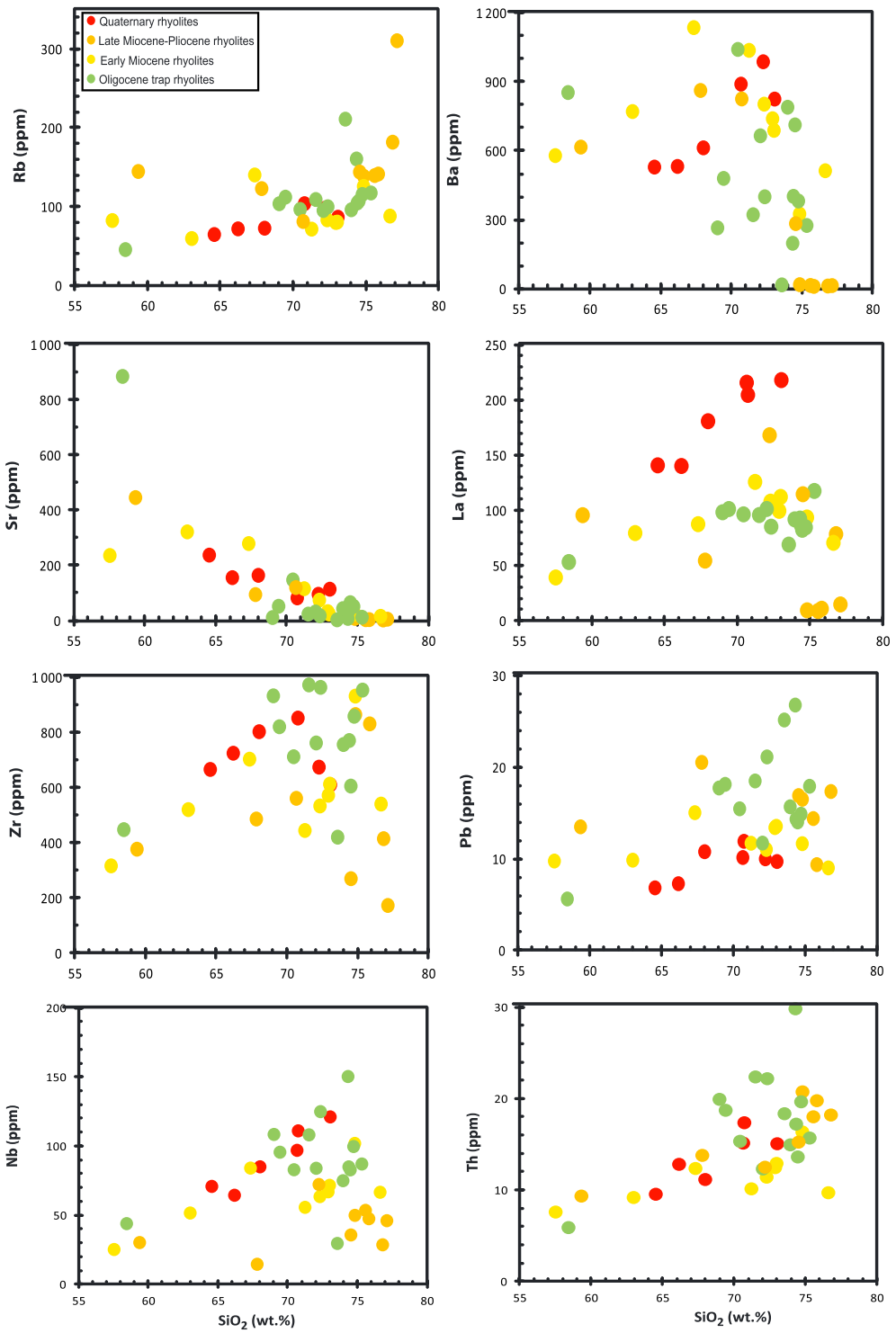

Figure 4. Variations of trace elements as a function of SiO_2 for marginal rhyolites from Western Afar. Symbols as Figure 2.

Strontium isotopes ratios were determined using a TIMS (Triton+, Thermo Scientific). Samples were loaded on Re filament, and five faraday cups are used in order to monitor Rb in the same time as Sr. Internal normalization using a $^{86}Sr/^{88}Sr$ ratio of 0.1194 and exponential law are used to correct for instrumental mass bias. Measurements of Nd isotope ratios were done using MC-ICPMS (see above). Instrumental

Geochemistry, Geophysics, Geosystems

10.1029/2018GC007446

Table 4

Sr, Nd, and Pb Isotopic Compositions of Rhyolites From Western Afar Segment

Sample	Age (Ma)	$^{87}Sr/^{86}Sr$	$^{87}Sr/^{86}Sr_I$	$^{143}Nd/^{144}Nd$	$^{143}Nd/^{144}Nd_I$	$^{206}Pb/^{204}Pb$	Err (2 s)	$^{206}Pb/^{204}Pb_I$	$^{207}Pb/^{204}Pb$	Err. (2 s)	$^{207}Pb/^{204}Pb_I$	$^{208}Pb/^{204}Pb$	Err. (2 s)	$^{208}Pb/^{204}Pb_I$
Quaternary Afar rhyolites														
AF13-30	0.52	0.704471 ± 12	*0.704449*	0.512795 ± 03	*0.512795*	18.307	0.001	*18.307*	15.567	0.001	*15.567*	38.359	0.005	*38.359*
AF13-25	0.10	0.703818 ± 10	*0.703816*	0.512868 ± 03	*0.512868*	18.542	0.001	*18.542*	15.565	0.001	*15.565*	38.584	0.005	*38.584*
AF15-17	2.50	0.703414 ± 09	*0.703386*	0.512931 ± 04	*0.512929*	18.556	0.001	*18.556*	15.562	0.001	*15.562*	38.602	0.005	*38.602*
AF15-19	2.50	0.703439 ± 06	*0.703392*	0.512956 ± 02	*0.512954*	18.583	0.001	*18.583*	15.536	0.001	*15.536*	38.623	0.005	*38.623*
AF15-11	1.32	0.703985 ± 11	*0.703944*	0.512868 ± 03	*0.512867*	18.574	0.001	*18.574*	15.574	0.001	*15.574*	38.774	0.005	*38.774*
AF13-340	1.30	0.704394 ± 19	*0.704328*	0.512844 ± 03	*0.512843*	18.513	0.001	*18.513*	15.570	0.001	*15.570*	38.706	0.005	*38.706*
AF15-10	0.56	0.703532 ± 09	*0.703517*	0.512936 ± 03	*0.512936*	18.733	0.001	*18.733*	15.560	0.001	*15.560*	38.778	0.005	*38.778*
Late Miocene-Pliocene margine synrift rhyolites (Bokeksa-Arabati section)														
AF12-15	4.00	0.706481 ± 15	*0.705618*	0.512741 ± 03	*0.512738*	18.511	0.001	*18.511*	15.562	0.001	*15.562*	38.207	0.005	*38.207*
Arabati-1	7.5	0.710727 ± 28	*0.706588*	0.512821	*0.512807*	18.431	0.0018	*18.416*	15.555	0.0020	*15.554*	38.125	0.007	*38.095*
Arabati-2	7.5	0.705461 ± 10	*0.705068*	0.512690	*0.512684*	18.358	0.0022	*18.342*	15.552	0.0020	*15.551*	38.029	0.007	*38.013*
Gainal-1	6.3	0.716155 ± 13	*0.705526*	0.512763	*0.512757*	18.391	0.0017	*18.378*	15.550	0.0017	*15.549*	37.920	0.004	*37.910*
Early Miocene margin synrift rhyolites (marginal graben dykes and Afar Finto section; Boksa-Arabati section)														
Hara-1	21.0	0.708419 ± 26	*0.705741*	0.512854 ± 08	*0.512839*	18.858	0.0021	*18.810*	15.586	0.002	*15.584*	38.546	0.005	*38.481*
Hara-2	22.6	0.705238 ± 13	*0.704672*	0.512895 ± 25	*0.512879*	18.851	0.0017	*18.788*	15.587	0.002	*15.584*	38.540	0.004	*38.476*
Hara-5	17.4	0.704340 ± 10	*0.704301*	0.512829 ± 15	*0.512816*	18.551	0.0022	*18.494*	15.570	0.002	*15.567*	38.297	0.005	*38.240*
Hara-6	17.4	0.705742 ± 24	*0.704959*	0.512678 ± 78	*0.512666*	18.872	0.0012	*18.827*	15.585	0.001	*15.582*	38.532	0.003	*38.473*
AF12-04	29	0.706311 ± 08	*0.704412*	0.512861 ± 04	*0.512838*	18.858	0.001	*18.791*	15.586	0.001	*15.583*	38.539	0.005	*38.477*
Oligocene prerift trap rhyolites (marginal graben and plateau)														
Hayk-1	29	0.707297 ± 22	*0.704734*	0.512864 ± 25	*0.512840*	18.973	0.002	*18.839*	15.596	0.002	*15.590*	38.613	0.005	*38.488*
Hayk-3	28.5	0.709945 ± 16	*0.705042*	0.512876 ± 03	*0.512852*	19.150	0.002	*19.058*	15.594	0.002	*15.590*	38.605	0.004	*38.492*
Arabati-4	29	0.705595 ± 15	*0.704824*	0.512821 ± 03	*0.512799*	18.728	0.002	*18.649*	15.593	0.001	*15.590*	38.620	0.004	*38.527*
Hayk-5	29	0.706808 ± 13	*0.705116*	0.512863 ± 04	*0.512841*	19.251	0.002	*19.110*	15.595	0.002	*15.589*	38.550	0.006	*38.416*
Kobo-1	29	0.708380 ± 17	*0.705011*	0.512843 ± 20	*0.512821*	19.064	0.001	*19.001*	15.585	0.001	*15.582*	38.624	0.003	*38.525*
Kobo-3	28.7	0.714978 ± 26	*0.705849*	0.512910 ± 04	*0.512889*	19.114	0.002	*19.017*	15.584	0.001	*15.580*	38.600	0.005	*38.495*
Kobo-8	29	0.723809 ± 17	*0.705334*	0.512898 ± 05	*0.512871*	19.237	0.001	*19.166*	15.595	0.001	*15.592*	38.574	0.001	*38.468*

Note. Italics define initial values.

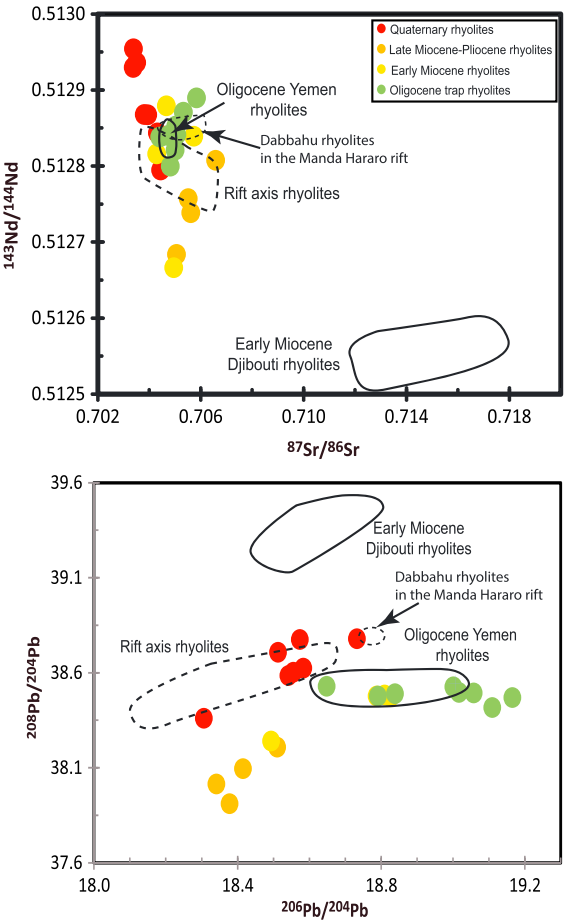

Figure 5. Variations of Sr-Nd-Pb isotopes for marginal rhyolites from Western Afar. Also shown for comparison are fields of rhyolites from Yemen (Baker et al., 2000), Djibouti (Deniel et al., 1994), and Ethiopian rift axis, both Afar (Hutchison et al., 2018) and MER (Giordano et al., 2014; Peccerillo et al., 2003).

mass bias was corrected using exponential law and internal normalization using $^{146}Nd/^{144}Nd$ of 0.7290 according to the previous methodology published by Luais et al. (1997). The admitted reference solution JNdi-1 (Tanaka et al., 2000) was used to check the methodology. In addition, the quality (accuracy and precision) of the process for Pb, Sr, and Nd was done by repeated dissolution of the international reference material BCR-1 ($^{206}Pb/^{204}Pb$ = 18.8193 ± 0.0025, $^{87}Sr/^{86}Sr$ = 0.705025 ± 0.000072, and $^{143}Nd/^{144}Nd$ = 0.512566 ± 0.000093 [2SD, n = 5]), and the blanks for the three systems were found negligible.

For zircon Helium dating, the samples were prepared at Service d'Analyse des Roches et des Minéraux (CRPG, Nancy, France) following the method described in Pik et al. (2003) and Tibari et al. (2016). Rocks were crushed and sieved, and heavy minerals were separated by densimetry. Aliquots of three to five zircon grains were prepared, and measurements of ^{4}He, U, Th, and Sm concentrations were performed on the same aliquots. Errors on age measurements are given by reproducibility on standards (Tibari et al., 2016) that is 6% on a 1-sigma interval of confidence. This level of precision is in agreement with those of the literature (see review in Tibari et al., 2016). The uncertainty is higher than for Ar-Ar datings, but it is still relevant to identify Cenozoic formations. On the other hand, the advantage of the U-Th-Sm/He method is that zircons are typically found in acid rocks, such as rhyolites. It is thus an ideal tool for mapping zones of large abundance of acid magmatism.

4. Results

4.1. U-Th-Sm/He Thermochronometry

U-Th-Sm/He ages of the marginal graben rhyolites are presented in Table 2. The trap rhyolites collected in Hayk and Kobo areas (Figure 1 and Table 1) situated within the present-day marginal graben yield U-Th-Sm/He ages ranging from 28.5 ± 1.7 Ma to 30.8 ± 1.8 Ma. These ages are in a close agreement with the previous U-Th-Sm/He ages of 29.7–30.6 Ma for strongly tilted rhyolites exposed in Sullu Adu area (Stab et al., 2016) and Rb-Sr isochron ages of 30.17 Ma for plateau rhyolites (Ayalew & Yirgu, 2003). U-Th-Sm/He thermochronometry gives two separate ages for Miocene felsic volcanism, one older lying between 17.4 ± 1.0 Ma and 23.45 ± 1.45 Ma and the other one younger ranging from 6.25 ± 0.35 Ma to 7.55 ± 0.50 Ma. There is no intermediate age between 7.6 and 17.4 Ma, indicating the episodic nature of the Miocene volcanism as it has been previously described elsewhere (Stab et al., 2016). Based on field location and correlation (Figure 1 and Table 1), the rhyolites emplaced near by the active magmatic segments have ages ranging from 0.1 to 4 Ma (Ferguson et al., 2013; Field et al., 2013; Lahitte et al., 2003; Stab et al., 2016). The ages obtained from this study allow us to subdivide the marginal rhyolites into four units: Oligocene trap rhyolites (28.5–30.8 Ma, ~30 Ma on average), early Miocene rhyolites (17.4–23.5 Ma, ~20 Ma on average), late Miocene-Pliocene rhyolites (between 8 and 4 Ma), and Quaternary rhyolites (2.5–0.1 Ma). We use this subdivision in the forthcoming discussion.

4.2. Major Elements

Bulk geochemical analyses of volcanic rocks from the western marginal graben, Ethiopian rift, are reported in Table 3. In the total alkalis-silica classification diagram (LeBas et al., 1986; Figure 2), the majority of the samples are rhyolite with minor trachytes. Most of the samples display a subalkaline affinity according to the alkaline/subalkaline delimitation of Irvine and Baragar (1971; Figure 2). Very few samples fall in the fields of basaltic trachyandesite (Hara 5), trachyandesite (AF13-73 and AF13-92), andesite (AF13-74), and dacite (AF15–17). For the sake of simplicity, we refer all the felsic samples hereafter to as rhyolite, which is the focus of this study. Harker variation diagrams are presented in Figure 3. With increasing SiO_2 content,

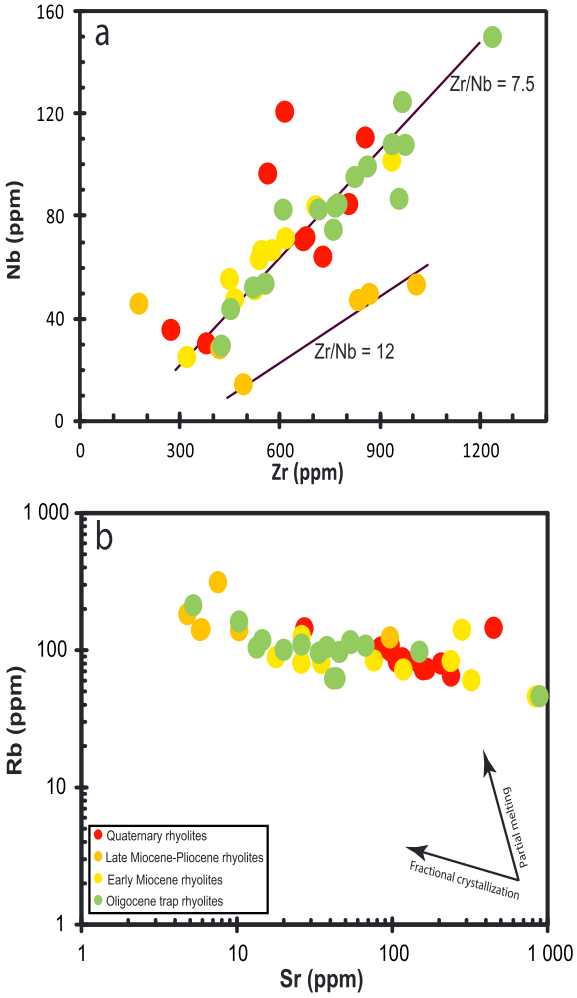

Figure 6. Bivariate plot of trace elements for marginal rhyolites from Western Afar. (a) Nb vs. Zr defining linear correlations that are an indicative of derivation from a broadly common source. (b) A log-log plot of Rb vs. Sr, displaying a wide variation in Sr concentration interpreted as crystallization-controlled origin for the rhyolites.

Fe_2O_3, TiO_2, and Al_2O_3 display negative correlation implying fractionation of Fe-, Ti-, and Al-bearing minerals such as olivine and clinopyroxene, Fe-Ti oxides, and plagioclase, respectively. Na_2O does not show a marked trend. The content of K_2O rises steadily, indicating its incompatible nature.

4.3. Trace Elements

The variations of trace elements against SiO_2 are shown in Figure 4. The concentrations of compatible trace elements such as V (not shown) and Sr steadily decrease with increasing SiO_2 content, reflecting fractionation of Fe-Ti oxides and plagioclase, respectively. Ba broadly shows negative correlation, though there are some scatterings. The concentrations of incompatible elements like Rb, Pb, and Th increase continuously throughout the suite. Other incompatible trace elements such as La, Nb, and Zr exhibit inflected trends at higher SiO_2 content in excess of 71 wt.%. The most evolved rhyolites with lower La, Nb, and Zr concentrations are characterized by higher contents of Rb and Th, simply related to the highly differentiated nature of these samples. The late Miocene rhyolites document depletion in light-REE (LREE; e.g., La) and high-field strength element (HFSE; e.g., Nb), providing evidence for crustal involvement in the genesis of these rhyolites or alternatively derivation from a depleted source.

4.4. Sr, Nd, and Pb Isotopes

Sr, Nd, and Pb isotopic compositions of volcanic rocks from the western portion of the Afar marginal graben are reported in Table 4. Initial Sr isotopic ratios show wide variation ranging from 0.7034 to 0.7066, with the highest values found in the late Miocene-Pliocene rhyolites. Initial $^{143}Nd/^{144}Nd$ ratios exhibit significant variation between 0.51267 and 0.51295, with the lowest values being recorded in the late Miocene-Pliocene rhyolites. Initial Pb isotopic ratios show considerable variations ($^{206}Pb/^{204}Pb$; 18.31–19.17, $^{207}Pb/^{204}Pb$; 15.55–15.59, $^{208}Pb/^{204}Pb$; 37.91–38.53), with the lowest ratios observed in the late Miocene- Pliocene rhyolites.

The Sr, Nd, and Pb isotopic compositions of the marginal rhyolites along with reference fields for rhyolites from the surrounding region are illustrated in Figure 5. In Sr-Nd isotopic space, the studied samples, except the Quaternary rhyolites, overlap significantly with the ranges of the Oligocene Yemen rhyolites (Baker et al., 2000) and young rift axis rhyolites (Giordano et al., 2014; Peccerillo et al., 2003), though they extend toward higher and lower $^{143}Nd/^{144}Nd$ values. In contrast, the Quaternary rhyolites as well as young rhyolites in the Manda Hararo rift (Hutchison et al., 2018) exhibit mantle-like $^{87}Sr/^{86}Sr$ and $^{143}Nd/^{144}Nd$ values. $^{87}Sr/^{86}Sr$ and $^{143}Nd/^{144}Nd$ ratios of early Miocene Djibouti rhyolites (Deniel et al., 1994) are distinct from those of the marginal rhyolites, implying that they contain a large crustal component.

In Pb-Pb isotopic space, the marginal rhyolites show two trends; one defined by Oligocene trap rhyolites forming a subhorizontal array at nearly constant $^{208}Pb/^{204}Pb$ of 38.4, respectively, and the other one by Miocene and Pliocene rhyolites of all ages displaying positive correlation. Modern rhyolites from Dabbahu volcano in the Manda Hararo rift segment (Hutchison et al., 2018) overlap with the range of the Quaternary rhyolites, but they cluster at the high $^{206}Pb/^{204}Pb$ end of the trend. Oligocene Yemen rhyolites share the same Pb-Pb isotopic range as the Oligocene trap rhyolites (Baker et al., 2000). Young rhyolites from the Ethiopian rift axis display distinct trend displaced toward the left of the marginal rhyolites (Giordano et al., 2014; Peccerillo et al., 2003). Pb-Pb isotopic values of early Miocene Djibouti rhyolites do not overlap with the range of the marginal rhyolites (Deniel et al., 1994), clearly indicating a strong contribution from upper crust in their genesis.

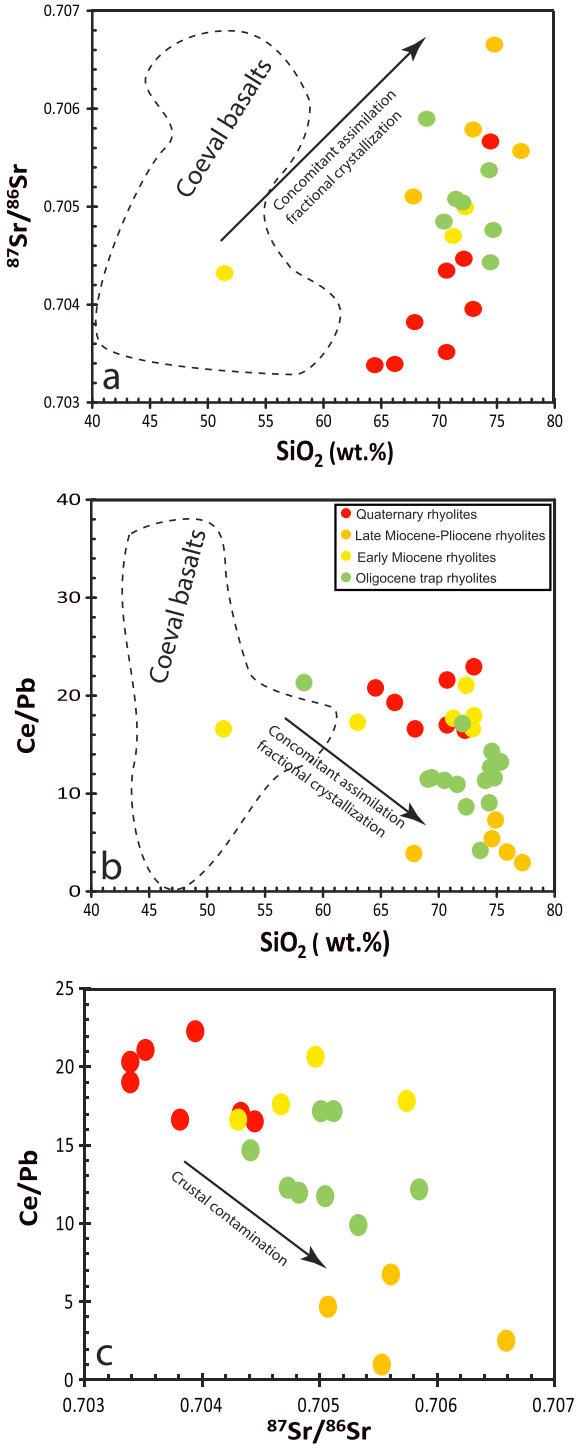

Figure 7. Variations of index of contamination, (a) $^{87}Sr/^{86}Sr$ and (b) Ce/Pb, as a function of index of differentiation (SiO_2) and (c) Ce/Pb against $^{87}Sr/^{86}Sr$ for marginal rhyolites from western Afar, showing good correlation accounted for in terms of crustal contamination. Also shown the ranges (shaded field) of the coeval basalts (Barrat et al., 1998; Deniel et al., 1994; Hart et al., 1989; Hutchison et al., 2018; Natali et al., 2016; Pik et al., 1999; Rooney et al., 2013; Vidal et al., 1991).

5. Discussion

5.1. Alteration

Although samples were collected for their freshness, we first track any chemical variation that may have been triggered by alteration. Macroscopically, most samples appear to be unaltered, but few samples have high LOI (loss on ignition) measurements occasionally reaching up to 4.3 wt.%, which may cause deuteric mobilization of fluid mobile elements. Furthermore, three samples show distinctly high contents of LOI (AF13-335: 4.8 wt.%, AF13-73: 5;5 wt.%, and AF13–337: 8.2 wt.%) relative to the rest of the series. There is a lack of correlation between LOI and any other major and trace elements, except Na_2O (not shown), indicating that deuteric alteration has not mobilized other elements and was probably insignificant.

5.2. Petrogenesis of the Rhyolites

The petrogenesis of the rhyolitic end member of a bimodal basalt-rhyolite suite is subject to a continuing debate. In some instances, chemical and isotopic data support an origin by low-pressure fractional crystallization of basaltic magma (e.g., Ayalew et al., 2002; Baker et al., 2000). In others, the lack of intermediate compositions appears to argue in favor of partial melting of crustal rocks instead (e.g., Davies & Macdonald, 1987; Macdonald et al., 1987). Despite this, systematic chemical and isotopic studies of the rhyolites are necessary to resolve the various arguments.

A fundamental issue in this study is to determine whether all the samples of the suite are linked to a common source by the same petrogenetic process or not. The first clue comes from the bivariate plots of incompatible trace element pairs (e.g., Nb vs. Zr; Figure 6a), whose bulk partition coefficients are very similar and will not vary both in the course of fractional crystallization and partial melting. It is evident that most of the samples define a strong linear trend regardless of their age, despite some dispersion. This supports the view that the marginal rhyolites were derived from a common source. Thus, the ratio of Zr/Nb ~7.5 approximates that in the source. Constancy of Zr/Nb ratios throughout the marginal rhyolites provides strong evidence that fractional crystallization has been the dominant process in their evolution as it is the only process that maintains unchanged ratios of incompatible trace elements in a suite of samples (e.g., Barberi et al., 1975). The only exceptions to this are the late Miocene rhyolites, which display a distinct linear array (with high Zr/Nb ~12), interpreted to indicate derivation from a depleted plume head source with higher Zr/Nb, as proposed for the associated Miocene basalts in Western Afar (between the marginal graben and Central Afar, Ferguson et al., 2010, 2013).

In addition, a log-log plot of highly incompatible trace element (e.g., Rb) against highly compatible trace element (e.g., Sr) in silicic melts is a viable tool to identify the likely physical processes, which account for the observed data variation (e.g., Halliday et al., 1991). On a Rb-Sr plot (Figure 6b), large changes in Sr concentrations are accompanied by limited changes in Rb abundances. Such trend is thought to reflect that the erupted magmas are related by fractional crystallization process. This model is more likely to produce the rhyolites in a short time span and minimizes crustal contamination relative to partial melting model. A similar interpretation is reached in the Ethiopian rift (both young Afar and MER volcanoes) where silicic magmas are thought to be generated through

Table 5
Isotopic Compositions and Concentrations of Sr, Nd, and Pb in Crustal and Basaltic Compositions

	Crust			Mantle
	C3	C6	C6*	Enriched Afar mantle plume
$^{87}Sr/^{86}Sr$	0.70863	0.72851	0.71	0.70375
Sr (ppm)	678	175	175	300
$^{143}Nd/^{144}Nd$	0.511368	0.512593	0.5129	0.51293
Nd (ppm)	34	23.5	23.5	20
$^{206}Pb/^{204}Pb$	17.625	18.85	19.3	18.8
Pb (ppm)	14	21.5	21.5	1.5

Note. C3; reworked craton lower crust (Davidson & Wilson, 1989), C6; differentiated juvenile Arabian-Nubian shield (Teklay et al., 2001), C6*; modified differentiated juvenile Arabian-Nubian shield (Teklay et al., 2001), Enriched Afar mantle plume (Pik et al., 1999).

protracted fractional crystallization processes of basalts (Field et al., 2013; Hutchison et al., 2016, 2018). Furthermore, field evidence indicates that the marginal rhyolites are often underlain by basalts. Such intimate stratigraphic relation between the basalts and rhyolites in a given volcanic field has been taken as a strong field evidence for crystallization-controlled origin for the rhyolites (e.g., Garland et al., 1995; Mahoney et al., 2008).

The derivation of the marginal rhyolites from parent basalt magmas through low-pressure crystal fractionation demands the presence at depth of extensive piles of complementary cumulates. As outlined before, the major element variations suggest that the fractionating phase assemblage controlling element partitioning consisted of olivine, clinopyroxene, plagioclase, and Fe-Ti oxides. This indicates that the cumulate rock has a bulk gabbroic composition, which contributes to the creation of new juvenile crust. We suggest that the volume of this cumulate can be several times greater than that of the erupted rhyolites, since >90% of crystallization is needed to reproduce the most evolved rhyolites. Our findings are supported by the existence of high *P* wave velocity (6.9–7.5 km/s; Bastow & Keir, 2011; Hammond et al., 2011) and positive Bouguer anomaly (δ = 3,000 g/cm^3; Tessema & Antoine, 2004) within the upper crust beneath Afar, inferred to be high-density mafic cumulates.

One of the objections to the fractional crystallization model is the scarcity of rocks of intermediate composition. Additionally, the origin of these rhyolites is paradoxical because their presumed immediate parental melt (trachyte), required to be even more voluminous, is generally sparse as an erupted magma type (Figure 2). Nevertheless, the Daly gap may either represent specific magma heat and water contents that triggers nonlinear crystal fractionation with cooling, inducing larger amount of primitive and evolved components compared to intermediate ones (Melekhova et al., 2013), or simply reflect the onset of significant amounts of Fe-Ti oxides fractionation, which can cause a rapid increase in SiO_2 content of the residual magma (Peccerillo et al., 1995, 2003). Indeed, many of these rhyolites contain microphenocrysts of Fe-Ti oxides, favoring fractionation of Fe-Ti oxides as a viable mechanism for the existence of SiO_2 gap in the volcanic records. Thus, the preservation of such a gap appears to be related to melt expulsion from a crystal mush as already first proposed by Marsh (2002) and then later supported by Bachmann and Bergantz (2004, 2008). This model predicts that only a small fraction (≤10 vol.%) of interstitial liquid is necessary to form the largest erupted rhyolites.

Two compelling evidences exist in the rock records, which favor for melt extraction from crystal mushes: (1) The crystal-poor Hayk rhyolite ignimbrite erupted concurrently (approximately 30 Ma) with crystal-rich Kobo porphyry rhyolite. (2) The Kobo and Hayk units exhibit similar geochemical affinity (i.e., similar incompatible trace element and isotopic ratios; Figures 5 and 6). These arguments suggest that the two units tapped a common, or similar *magma chamber* though they are about 100 km far apart from each other. The fact that the occurrences of coeval crystal-poor and crystal-rich magmas (chronological proximity and geochemical affinity) within the volcanic record of the marginal graben provide strong support to the idea that the silicic melts squeezed out from the crystal mushes by compaction. Hence, the crystal-poor Hayk ignimbrite is interpreted as the evolved cap of the crystal-rich Kobo rhyolite, now exposed on the surface most likely by erosion.

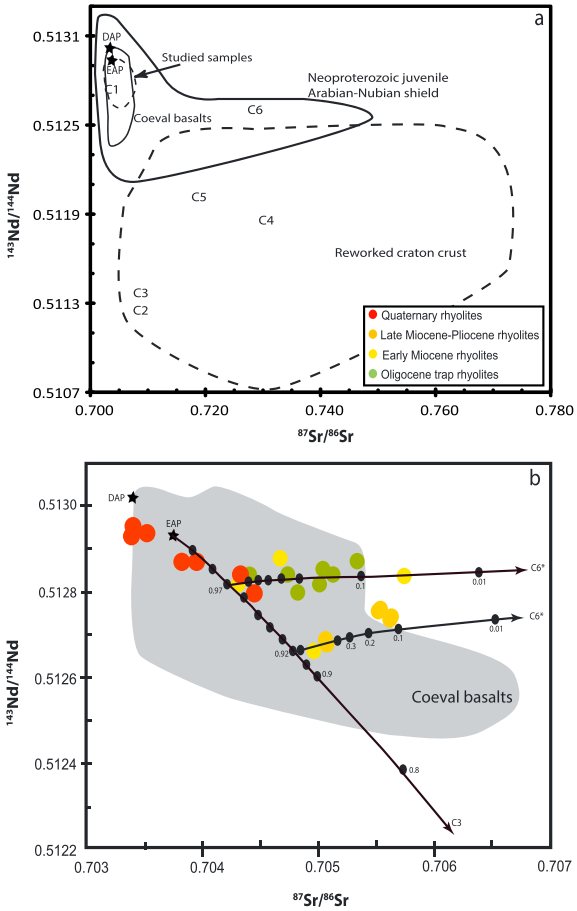

Figure 8. (a) Sr-Nd isotopic variations of the studied samples compared with those of the associated basalts (Barrat et al., 1998; Deniel et al., 1994; Hart et al., 1989; Hutchison et al., 2018; Natali et al., 2016; Pik et al., 1999; Rooney et al., 2013; Vidal et al., 1991) and the crust (Bailoa et al., 2003; Baker et al., 2000; Davidson & Wilson, 1989; Küster et al., 2008; Lucassen et al., 2008; Stern & Abdelsalam, 1998; Teklay et al., 2001) from the region. C1, C2, C3, C4, C5, and C6 are true representatives of the upper and lower crust chosen to consider the various trajectories. Although there is a tendency to have little overlap, the Neoproterozoic juvenile Arabian-Nubian shield is considerably characterized by higher $^{143}Nd/^{144}Nd$ ratio than the reworked craton crust. The Neoproterozoic juvenile Arabian-Nubian shield also displays a wide range of Nd isotopic composition, which encompasses the ranges of the basalts and rhyolites, but it possesses marked troughs at Nb-Ta in mantle-normalized multielement variation diagram (e.g., Woldemichael et al., 2010). (b) Zoom in of Figure 8a to show a two-stage AFC model involving small degrees (3–8%, $r = 0.6$) of crystallization of the more primitive magmas at deep levels, followed by greater degrees (90%, $r = 0.15$) of fractionation at higher levels. Marks on the AFC curves indicate fraction of residual magma. Bulk distribution coefficient; D_{Sr} (0.037–0.976) and D_{Nd} (0.158–0.658) are from Rollinson (1993). DAP; depleted Afar mantle plume, EAP; enriched Afar mantle plume, C3; reworked craton lower crust, C6*; modified differentiated juvenile Arabian-Nubian shield upper crust.

5.3. Open System Evolution

The trace element and Sr-Nd-Pb isotope features of the marginal rhyolites provide ample evidence for the involvement of crustal rocks in their genesis. It has become apparent that ratios of highly incompatible trace elements (e.g., Ce/Pb) and radiogenic isotopes (e.g., $^{87}Sr/^{86}Sr$) may help to track crustal involvement in silicic melts. Plots of $^{87}Sr/^{86}Sr$ (Figure 7a) and Ce/Pb (Figure 7b) versus SiO_2 depict good correlation, suggesting that concomitant assimilation-fractional crystallization (AFC) style of crustal contamination has played a role in the genesis and evolution of the marginal rhyolites. Similarly, in a plot of Ce/Pb against Sr isotope ratio (Figure 7c), samples with low Ce/Pb ratio are characterized by high $^{87}Sr/^{86}Sr$ value, accounted for in terms of crustal contamination. The recent Afar rhyolites appear to be less contaminated than the rest of the rhyolites from the margin and plateau and share the same isotopic composition (and the same amount of contamination) as the contemporaneous basalts.

Sr, Nd, and Pb isotopic compositions are used to assess further the nature and extent of contamination as they distinctly depict the fields of the mantle and the crust. One point worth mentioning is the lack/absence of Pb isotopic composition on the Arabian-Nubian shield underlying the volcanic rocks below Ethiopia. This makes the AFC calculations to be less reliable. Nevertheless, we used the available data from the surrounding region in Sudan (Bailoa et al., 2003; Davidson & Wilson, 1989), Egypt (Küster et al., 2008; Lucassen et al., 2008; Stern & Abdelsalam, 1998), Eritrea (Teklay et al., 2001), and Yemen (Baker et al., 2000), which show a wide range of isotopic compositions for the crust in this area. Owing to the highly variable isotopic compositions of the basement, the composition of the crustal end-member representing the contaminant is poorly constrained.

Trace element and isotope (especially Pb) data place valuable constraints on the approximate environment of crustal contamination (i.e., upper versus lower crust) in the petrogenesis of the studied samples. The most contaminated samples, those with the highest Sr isotopic composition and the lowest Ce/Pb ratio, are the Oligocene trap and the late Miocene-Pliocene rhyolites. As shown on Figure 5, the Oligocene rhyolites have the highest $^{206}Pb/^{204}Pb$, while some Quaternary rhyolites have $^{206}Pb/^{204}Pb$ ratio as low as those for the late Miocene-Pliocene rhyolites. The high Pb isotope composition of the Oligocene trap rhyolites seems to indicate contamination by the upper crust, while for the late Miocene-Pliocene rhyolites their low Pb isotope composition indicates a lower crust-dominant fingerprint. On the other hand, the late Miocene-Pliocene samples show relative enrichment in Rb and Th (Figure 4 and Table 4), a distinctive signature of the upper crust. Decoupling of trace element and Pb isotope systematics in the late Miocene-Pliocene rhyolites can be interpreted in terms of multiple levels of magma interactions within the crust. In such scenario, differentiation might have occurred first at depth (hot wall rock, high r; where r is the ratio of rates of assimilation to crystallization), and then at shallow crustal levels (cold wall rock, low r) with a change in the composition of the assimilated material. Since the difference between low Pb isotopic ratio and high Th content is not observed in the trap rhyolites, only one step model explains the AFC process.

AFC modeling (DePaolo, 1981) is attempted using the available Sr-Nd-Pb isotopic data to quantify the extent of contamination in the marginal rhyolites. The mantle and crust end-members considered in the model are reported in Table 5. The contaminants selected to reproduce the different Sr-Nd-Pb isotopic trends of the

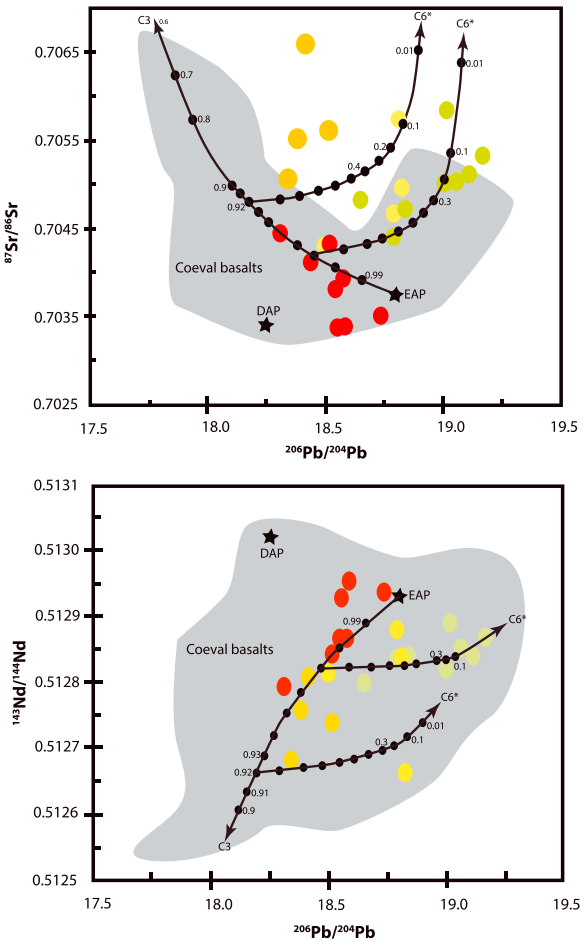

Figure 9. $^{87}S/^{86}Sr$ and $^{143}N/^{144}Nd$ plotted against $^{206}Pb/^{204}Pb$, with model AFC curves of varying *r* calculated as Figure 8b. Marks on the AFC curves indicate fraction of residual magma. Bulk distribution coefficient; D_{Sr} (0.037–0.976), D_{Nd} (0.158–0.658) and D_{Pb} (0.003–0.361) are from Rollinson (1993). C3; reworked craton lower crust.

rhyolites. In the contrary, only a single starting basalt composition (*Enriched Afar Plume* composition) considered through 30 Ma of AFC process. The choice of this starting composition for 30 Ma of AFC modeling is based on the fact that all the noncontaminated basalts, from the Oligocene trap to the recent Afar rift segments, exhibit similar isotopic compositions (e.g., Ferguson et al., 2010, 2013; Hutchison et al., 2018). This suggests that all the associated basalt magmas had the same primary composition before differentiation and contamination over the 30 Ma of magmatism in the area.

The results of AFC modeling are illustrated in Figures 8 and 9. Chemical and isotopic data support an origin by open system evolution at different levels within the crust. In early stages of differentiation, the more primitive magmas, generated within the enriched Afar mantle plume, interact with the lower crust (up to 8% crystallization, 5% contamination) at a fairly high rate ($r = 0.6$). At later stages of fractionation, which produced the rhyolites, the evolved, and contaminated magmas differentiate at higher levels and are contaminated by upper crust (up to 90% crystallization, 14% contamination) probably at a lesser rate ($r = 0.15$). The initial high-*r* stage is required in the petrogenesis of these magmas to account for the observed significant amount of contamination (up to 5%) acquired during rather limited evolution of the primary magmas in the basaltic field of compositions. Such an early high-*r* stage of AFC has been demonstrated to be a common feature of initial basalt contamination due to specific thermal constraints (Reiners et al., 1995). The crustal contaminant used in the model for the upper crust is not a real basement sample from the region. Indeed, a lot of the upper crustal end-members considered elsewhere could be compatible with such AFC evolution for Sr and Pb isotopes, but the observed trends on Figures 8 and 9 require an isotopic end member with slightly higher Nd isotopic ratio than what has been measured in basement surrounding the Ethiopian volcanic province. We then propose such a composition compatible with the surrounding record and the isotopic trends as upper crustal contaminant for these magmas (C6*). Over all, the different Sr-Nd-Pb trajectories of the investigated rhyolites can be satisfactorily explained by assimilation of heterogeneous crust in two distinct and sequential steps first in the lower crust, and later in the upper crust.

It is important to note that the amount of contamination is different and higher for all the rhyolites than the basalts, except those from Afar, which appear to remain similarly to the associated basalts, and mostly affected by the first step of contamination that occurs within the lower crust (Figures 8b and 9). Moreover, the isotopic trends of the rhyolites appear anchored at the end of those described by the basalts, as it is proposed in our two steps AFC model. Such cogenetic evolution of the basalts and rhyolites via AFC processes during differentiation in the lower crust implies that the observed isotopic trends are controlled by two distinct types of end-members, which are the Afar Mantle Plume (as source of primitive melts) and two crustal components (as sources of contamination). This interpretation of the Sr-radiogenic components is opposed to the alternative view that such isotopic trends results from participation of an Enriched Mantle component (EM type) that could originate in the lithospheric mantle (Rooney et al., 2012). The immediate implication of this interpretation is that rhyolitic magmas can be used to discriminate crustal contamination of mantle-derived magmas from enriched lithospheric mantle sources (Furman et al., 2016; Rooney et al., 2012). Thus, for a suite of lavas, rhyolitic magmas may help to identify some of the ambiguous geochemical variations observed within the associated basalts.

5.4. Temporal Evolution of Contamination and Geodynamic Implications

Felsic samples studied herein range in age from ~30 Ma (prerift) to ~0.1 Ma, documenting most of the volcano-tectonic events that occurred successively in the area. Compositional variations of these rocks

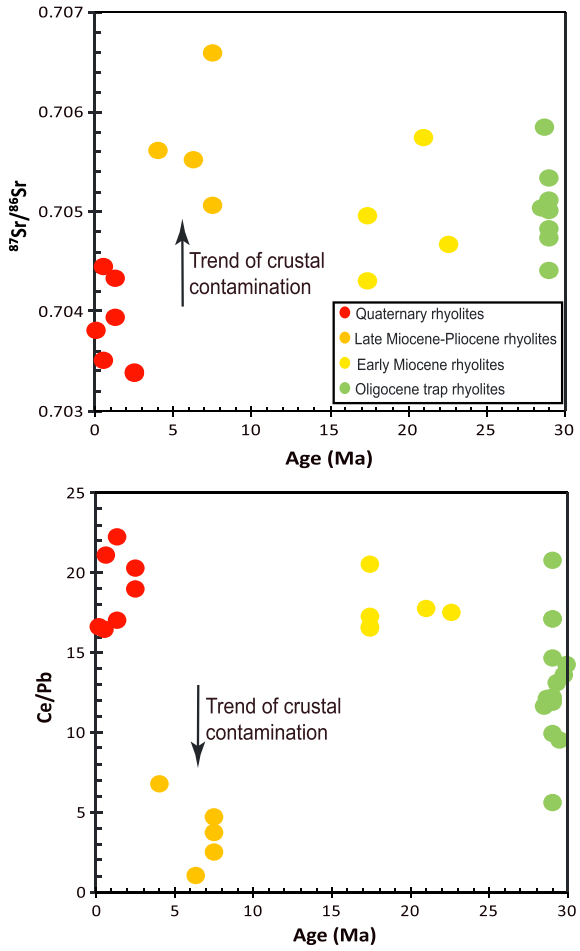

Figure 10. Temporal compositional variations of the marginal rhyolites, demonstrating that the extents of contamination tend to increase as rifting progressed.

with time are shown in Figure 10. Oligocene trap rhyolites (erupted prior to the onset of rifting) are contaminated to some extent, while early Miocene rhyolites (emplaced during incipient rifting) show less evidence for crustal contamination. Late Miocene-Pliocene rhyolites, related to the thinning of the crust, are highly contaminated. In the contrary, Quaternary rhyolites (emplaced as rifting progressed to continental breakup) appear to be uncontaminated. $^{87}Sr/^{86}Sr$ and Ce/Pb values indicate that crustal involvement was significant in the late Miocene-Pliocene rhyolites extruded across the rifted zones, as exemplified by relatively high $^{87}Sr/^{86}Sr$ and low Ce/Pb values. It is important to note that these rhyolites are the most differentiated rocks (with SiO_2 content of 75–77 wt.%) and show the highest degree of crustal contamination. Indeed, further differentiation suggests longer periods of residence in crustal magma chambers, which could elevate the amount of crustal contamination. Alternatively, the late Miocene-Pliocene rhyolites originated from differentiation of depleted basalts, derived from a depleted source in the Afar plume head (Barrat et al., 2003), which can have enhanced the impact of contamination on trace element and isotopic ratios for equivalent amount of crustal assimilation (the contamination degree estimate therefore probably represents a maximum value).

On Figure 10, it is clear that the role of crustal involvement in the genesis of the studied rhyolites appears to be related to the stage of crustal extension. This is particularly the case for the Quaternary rhyolites, emplaced nearby the active magmatic segments during the breakup stage of rifting, which exhibit $^{87}Sr/^{86}Sr$ and Ce/Pb values that are indistinguishable from those of the cogenetic Central Afar segment basalts (Hutchison et al., 2018). This suggests that the second stage of upper crustal contamination, which modifies strongly Sr isotopic composition (Figures 8 and 9), is absent for these magmas, and therefore, that the rhyolites from Afar only suffered the same contamination process as the basalts, that is, the first stage in the lower crust. Such a characteristic is compatible with the long-lived ideas and hypotheses (Hammond et al., 2011; Stab et al., 2016) that the Afar crust has been massively intruded by juvenile magmas in the course of rifting (especially after the Stratoïde Fm. emplacement,

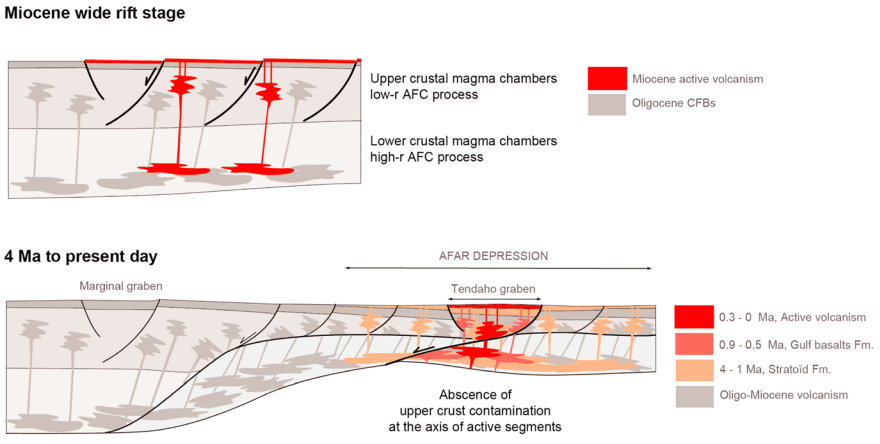

Figure 11. Magma plumbing system evolution in the course of margin extension. Equilibrated cross-sections are based on Stab et al. (2016). Drawing has been simplified to allow better representation of the magmatic plumbing system during the two selected periods of Miocene and 4–0 Ma recent volcanism. The represented unit for Oligocene and Miocene volcanism exhibit internal architecture with differential sea-ward tilted volcanic levels, up to 60° for the lower units of the lava pile.

Figure 11) and is now at a transitional stage between continental rifting and oceanic accretion. Indeed, differentiation of magmas in such a heavily intruded crust can still be accompanied by assimilation of country rock, yet its mostly juvenile nature will prevent significant modifications of trace elements and radiogenic isotopes signatures. On the other hand, the first stage of contamination at lower crustal levels is still identified in the geochemical data, which testifies that some lower crust may still be present around the associated plumbing system. Alternatively, as proposed by Barrat et al. (1993, 1998, 2003) for various segments in Afar, the Afar rhyolites contamination may be related to interaction of magmas (rhyolites and possibly basalts) with previously hydrothermally altered juvenile crust. This alternate model suggests the possibility that Afar rift segments may be associated with an entirely juvenile crust. The distinction between those two models (i.e., interaction with lower continental crust versus interaction with hydrothermally altered juvenile crust) cannot be done with the data presented herein and will necessitate further studies.

Following the recent crustal structure proposed for Central Afar and adjacent areas by Stab et al. (2016), we combine all these arguments in a model highlighting two specific stages (Figure 11). During early Miocene, the rifting was wide and associated with discrete volcanic phases (Figure 11). At the end of this stage, the Afar crust experienced a main thinning event leading to the emplacement of the voluminous Stratoïde Fm. (Stab et al., 2016). Since then, the divergence has localized in the present-day magmatic segments (such as Manda Hararo) (Figure 11) where the crustal structure results from (i) important addition of juvenile basic magmas and (ii) preferential removal of the upper crust along the detachment faults that accommodated divergence. Such results and interpretations suggest that the present-day Central Afar is very close to continental breakup, which will be achieved once the continental crust will be entirely replaced by new magmatic crust.

6. Conclusions

Rhyolites from western marginal graben down to the Central Afar range in age from ~30 Ma (prerift stage), ~20 Ma (early synrift), ~8–4 Ma (main thinning event) to ~2.5–0.1 Ma (late synrift), representing the whole volcano-tectonic events that occurred successively. These rhyolites are geochemically similar and are spatially associated with basalts over the entire eruptive period. The compositions of the rhyolites are best explained by protracted differentiation at different levels within the crust. Such evolution involves small degrees (up to 8%, 5% contamination) of crystallization of parental liquids at a fairly high assimilation/crystallization rate in the lower crust (r = 0.6), followed by greater degrees (90%, 14% contamination) of fractionation of evolved magmas in the upper crust to produce the rhyolites probably at a lesser rate (r = 0.15). The Quaternary rhyolites, emplaced toward the final stage of rifting, record little interactions with the crust with isotopic signatures compatible with contamination limited to the first step in the lower crust, or alternatively to interactions with previously hydrothermally altered juvenile crust. This is compatible with the fact that the present-day crust below the active magmatic segments is transitional. This suggests that rifting is almost achieved close to continental breakup, which will be achieved once the continental crust will be entirely replaced by new magmatic crust. Rhyolite magmas emitted over the last 30 Ma display very similar signatures (or contamination degree) for a given period. This implies that the plumbing system and magma interactions with host rocks are mainly governed by the regional tectonic regime, and crust architecture.

Acknowledgments
Dereje Ayalew is grateful to the French Embassy in Ethiopia for offering SSHN (Séjours Scientifiques de Haut Niveau) travel grants. Part of this work was funded by the French Action Marges program. The authors thank Gilles Chazot and anonymous reviewer and Editor Marie Edmonds for their detailed and constructive comments and suggestions that amend the quality of the manuscript. Data presented in this paper are contained within the manuscript.

References

Annen, C., Blundy, J., & Sparks, R. S. J. (2006). The genesis of intermediate and silicic magmas in deep crustal hot zones. *Journal of Petrology*, *47*, 505–539.

Annen, C., & Sparks, R. S. J. (2002). Effects of repetitive emplacement of basaltic intrusions on thermal evolution and melt generation in the crust, Earth Planet. *Science Letters*, *203*, 937–955.

Ayalew, D., Barbey, P., Marty, B., Reisberg, L., Yirgu, G., & Pik, R. (2002). Source, genesis, and timing of giant ignimbrite deposits associated with Ethiopian continental flood basalts. *Geochimica et Cosmochimica Acta*, *66*, 1429–1448.

Ayalew, D., Ebinger, C., Bourdon, E., Wolfenden, E., Yirgu, G., & Grassineau, N. V. (2006). Temporal compositional variation of syn-rift rhyolites along the western margin of the southern Red Sea and northern main Ethiopian rift. In G. Yirgu, C. J. Ebinger, & P. K. H. Maguire (Eds.), *The Afar volcanic province within the east African rift system*, *Geol. Soc. Spec. Publ.*, (Vol. 259, pp. 121–130).

Ayalew, D., & Yirgu, G. (2003). Crustal contribution to the genesis of Ethiopian plateau rhyolitic ignimbrites: basalt and rhyolite geochemical provinciality. *Journal of the Geological Society London*, *160*, 47–56.

Bachmann, O., & Bergantz, G. W. (2004). On the origin of crystal-poor rhyolites: extracted from batholithic crystal mushes. *Journal of Petrology*, *45*, 1563–1585.

Bachmann, O., & Bergantz, G. W. (2008). Rhyolites and their source mushes across tectonic settings. *Journal of Petrology*, *49*, 2277–2285.

Bailoa, T., Schandelmeier, H., Franz, G., Sun, C.-H., & Stern, R. J. (2003). Plutonic and metamorphic rocks from the Keraf Suture (NE Sudan): A glimpse of Neoproterozoic tectonic evolution on the NE margin of W. Gondwana. *Precambrian Research*, *123*, 67–80.

Baker, J. A., Macphrson, C. G., Menzies, M. A., Thirlwall, M. F., Al-Kadasi, M., & Mattey, D. P. (2000). Resolving crustal and mantle contributions to continental flood volcanism, Yemen: Constraints from mineral oxygen isotope data. *Journal of Petrology*, *41*, 1805–1820.

Baker, J. A., Snee, L., & Menzies, M. A. (1996). A brief period of Oligocene flood volcanism in western Yemen: implications for the duration and rate of continental flood volcanism at the Afro-Arabian triple junction. *Earth and Planetary Science Letters*, *138*, 39–56.

Barberi, F., Ferrara, G., Santacroce, R., Treuil, M., & Varet, J. (1975). A transitional basalt-pantellerite sequence of fractional crystallization, the Boina Centre (Afar Rift, Ethiopia). *Journal of Petrology*, *16*, 22–56.

Barrat, J. A., Fourcade, S., Jahn, B. M., Cheminée, J. L., & Capdevila, R. (1998). Isotope (Sr, Nd, Pb, O) and trace-element geochemistry of volcanics from the Erta'Ale range (Ethiopia). *Journal of Volcanology and Geothermal Research*, *80*, 85–100.

Barrat, J. A., Jahn, B. M., Fourcade, S., & Joron, J. L. (1993). Magma genesis in an ongoing rifting zone: The Tadjoura Gulf. *Geochimica et Cosmochimica Acta*, *57*, 2291–2302.

Barrat, J. A., Joron, J. L., Taylor, R. N., Fourcade, S., Nesbitt, R. W., & Jahn, B. M. (2003). Geochemistry of basalts from Manda Hararo, Ethiopia: LREE-depleted basalts in Central Afar. *Lithos*, *69*, 1–13.

Bastow, I., & Keir, D. (2011). The protracted development of the continent-ocean transition in Afar. *Nature Geoscience*, *4*, 248–250.

Bohrson, W. A., & Reid, M. R. (1997). Genesis of peralkaline volcanic rocks in an ocean island setting by crustal melting and open-system processes: Socorro Island, Mexico. *Journal of Petrology*, *38*, 1137–1166.

Cameron, K. L., Parker, D. F., & Sampson, D. E. (1996). Testing crustal melting models for the origin of flood rhyolites: A Nd–Pb–Sr isotopic study of the Tertiary Davis Mountains volcanic field, west Texas. *Journal of Geophysical Research*, *101*, 20,407–20,422.

Davidson, J. P., & Wilson, I. R. (1989). Evolution of an alkali basalt-trachyte suite from Jebel Marra volcano, Sudan, through assimilation and fractional crystallization. *Earth and Planetary Science Letters*, *95*, 141–160.

Davies, G. R., & Macdonald, R. (1987). Crustal influences in the petrogenesis of the Naivasha basalt-comendite complex: Combined trace element and Sr-Nd-Pb constraints. *Journal of Petrology*, *28*, 1009–1031.

Deniel, C., Vidal, P., Coulon, C., Vellutini, P., & Piguet, P. (1994). Temporal evolution of mantle sources during continental rifting: The volcanism of Djibouti (Afar). *Journal of Geophysical Research*, *99*, 2853–2869.

DePaolo, D. J. (1981). Trace element and isotopic effects of combined wall-rock assimilation and fractional crystallization. *Earth and Planetary Science Letters*, *53*, 189–202.

Doubre, C., Manighetti, I., Dorbath, C., Dorbath, L., Jacques, E., & Delmond, J.-C. (2007). Crustal structure and magmato-tectonic processes in an active rift (Asal-Ghoubbet, Afar, East Africa): 1. Insights from a 5-month seismological experiment. *Journal of Geophysical Research*, *112*, B05405. https://doi.org/10.1029/2005JB003940

Dugda, M., Nyblade, A., Julia, J., & Ammon, C. (2005). Crustal structure in Ethiopia and Kenya from receiver function analysis: Implications for rift development in eastern Africa. *Journal of Geophysical Research*, *110*, B01303. https://doi.org/10.1029/2004JB003065

Ebinger, C., & Casey, M. (2001). Continental breakup in magmatic provinces: An Ethiopian example. *Geology*, *29*, 527–530.

Ebinger, C. J., Yemane, T., WoldeGabriel, G., Aronson, J. L., & Walter, R. C. (1993). Late Eocene-Recent volcanism and faulting in the southern main Ethiopian rift. *Journal of the Geological Society of London*, *150*, 99–108.

Ferguson, D. J., Barnie, T. D., Pyle, D. M., Oppenheimer, C., Yirgu, G., Lewi, E., Kidane, T., et al. (2010). Recent rift-related volcanism in Afar, Ethiopia. *Earth and Planetary Science Letters*, *292*, 409–418.

Ferguson, D. J., Calvert, A. T., Pyle, D. M., Blundy, J. D., Yirgu, G., & Wright, T. J. (2013). Constraining timescales of focused magmatic accretion and extension in the Afar crust using lava geochronology. *Nature Communications*, *4*, 14–16.

Field, L., Blundy, J., Calvert, A., & Yirgu, G. (2013). Magmatic history of Dabbahu, a composite volcano in the Afar rift, Ethiopia. *Geological Society of America Bulletin*, *125*, 128–147.

France, L., Demacon, M., Gurenko, A. A., & Briot, D. (2016). Oxygen isotopes reveal crustal contamination and a large, still partially molten magma chamber in Chaîne des Puys (French Massif Central). *Lithos*, *260*, 328–338.

France, L., Koepke, J., Ildefonse, B., Cichy, S., & Deschamps, F. (2010). Hydrous partial melting in the sheeted dike complex at fast spreading ridges: Experimental and natural observations. *Contributions to Mineralogy and Petrology*, *160*, 683–704.

France, L., Koepke, J., MacLeod, C. J., Ildefonse, B., Godard, M., & Deloule, E. (2014). Contamination of MORB by anatexis of magma chamber roof rocks: constraints from a geochemical study of experimental melts and associated residues. *Lithos*, *202–203*, 120–137.

Furman, T., Wendy, W. R., & Elkins-Tanton, L. T. (2016). Evolution of the east African rift: drip magmatism, lithospheric thinning and mafic volcanism. *Geochimica et Cosmochimica Acta*, *185*, 418–434.

Garland, F., Hawkesworth, C. J., & Mantovani, M. S. M. (1995). Description and petrogenesis of the Paraná rhyolites, southern Brazil. *Journal of Petrology*, *36*, 1193–1227.

Geist, D., Howard, K. A., & Larson, P. (1995). The generation of oceanic rhyolites by crystal fractionation: the basalt-rhyolite association at Volcán Alcedo, Galápagos Archipelago. *Journal of Petrology*, *36*, 965–982.

George, R., Rogers, N., & Kelley, S. (1998). Earliest magmatism in Ethiopia: Evidence for two mantle plumes in one flood basalt province. *Geology*, *26*, 923–926.

Giordano, F., D'Antonio, M., Civetta, L., Tonarini, S., Orsi, G., Ayalew, D., Yirgu, G., et al. (2014). Genesis and evolution of mafic and felsic magmas at Quaternary volcanoes within the main Ethiopian rift: insights from Gedemsa and Fanta'Ale complexes. *Lithos*, *188*, 130–144.

Halliday, A. N., Davidson, J. P., Hildreth, W., & Holden, P. (1991). Modelling the petrogenesis of high Rb/Sr silicic magmas. *Chemical Geology*, *92*, 107–114.

Hammond, J. O. S., Kendall, J. M., Stuart, G. W., Keir, D., Ebinger, C., Ayele, A., & Belachew, M. (2011). The nature of the crust beneath the Afar triple junction: evidence from receiver functions. *Geochemistry, Geophysics, Geosystems*, *2*, Q12004. https://doi.org/10.1029/2011GC003738

Hart, W., WoldeGabriel, G., Walter, R., & Mertzman, S. (1989). Basaltic volcanism in Ethiopia: constraints on continental rifting and mantle interactions. *Journal of Geophysical Research*, *94*, 7731–7748.

Hayward, N., & Ebinger, C. (1996). Rift kinematics and along-axis segmentation in northern Afar. *Tectonics*, *15*, 244–257.

Hofmann, C., Courtillot, V., Féraud, G., Rochette, P., Yirgu, G., Ketefo, E., & Pik, R. (1997). Timing of the Ethiopian flood basalt event and implications for plume birth and global change. *Nature*, *389*, 838–841.

Hutchison, W., Mather, T. M., Pyle, D. M., Boyce, A. J., Gleeson, M. L. M., Yirgu, G., Blundy, J. D., et al. (2018). The evolution of magma during continental rifting: New constraints from the isotopic and trace element signatures of silicic magmas from Ethiopian volcanoes. *Earth and Planetary Science Letters*, *489*, 203–218.

Hutchison, W., Pyle, D. M., Mather, T. A., Yirgu, G., Biggs, J., Cohen, B. E., Barfod, D. N., et al. (2016). The eruptive history and magmatic evolution of Aluto volcano: new insights into silicic peralkaline volcanism in the Ethiopian rift. *Journal of Volcanology and Geothermal Research*, *328*, 9–33.

Irvine, T., & Baragar, W. (1971). A guide to the chemical classification of the common volcanic rocks. *Canadian Journal of Earth Sciences*, *8*, 523–548.

Kidane, T., Courtillot, V., Manigehetti, I., Audin, L., Lahitte, P., Quidelleur, X., Gillot, P. Y., et al. (2003). New paleomagnetic and geochronologic results from Ethiopian Afar: Block rotations linked to rift overlap and propagation and determination of a ~2 Ma reference pole for stable Africa. *Journal of Geophysical Research*, *108*(B2), 2102. https://doi.org/10.1029/2001JB000645

Kogan, L., Fisseha, S., Bendick, R., Reilinger, R., McClusky, S., King, R., & Solomon, T. (2012). Lithospheric strength and strain localisation in continental extension from observations of the East African Rift. *Journal of Geophysical Research*, *117*, B03402. https://doi.org/10.1029/2011JB008516

Küster, D., Liégeois, J. P., Matukov, D., Sergeev, S., & Lucassen, F. (2008). Zircon geochronology and Sr, Nd, Pb isotope geochemistry of granitoids from Bayuda Desert and Sabaloka (Sudan): Evidence for a Bayudian event (920–900 Ma) preceding the Pan-African orogenic cycle (860–590 Ma) at the eastern boundary of the Saharan Metacraton. *Precambrian Research*, *164*, 16–39.

Lahitte, P., Gillot, P., & Courtillot, V. (2003). Silicic central volcanoes as precursors to rift propagation: The Afar case. *Earth and Planetary Science Letters*, *207*, 103–116.

LeBas, M., LeMaitre, R., Streckeisen, A., & Zanettin, B. (1986). A chemical classification of volcanic rocks based on the total alkali-silica diagram. *Journal of Petrology*, *27*, 745–750.

Leroy, S., Razin, P., Autin, J., Bache, F., d'Acremont, E., Watremez, L., Robinet, J., et al. (2012). From rifting to oceanic spreading in the Gulf of Aden: A synthesis. *Arabian Journal of Geosciences*, *5*, 859–901.

Luais, B., Telouk, P., & Albarède, F. (1997). Precise and accurate neodymium isotopic measurements by plasma-source mass spectrometry. *Geochimica et Cosmochimica Acta*, *61*, 4847–4854.

Lucassen, F., Franz, G., Romer, R. L., Pudlo, D., & Dulski, P. (2008). Nd, Pb, and Sr isotope composition of Late Mesozoic to Quaternary intraplate magmatism in NE-Africa (Sudan, Egypt): High-μ signatures from the mantle lithosphere. *Contributions to Mineralogy and Petrology*, *156*, 765–784.

Macdonald, R. (2012). Evolution of peralkaline silicic complexes: Lessons from the extrusive rocks. *Lithos*, *152*, 11–22.

Macdonald, R., Davies, G. R., Bliss, C. M., Leat, P. T., Bailey, D. K., & Smith, R. L. (1987). Geochemistry of high-silica peralkaline rhyolites, Naivasha, Kenya Rift Valley. *Journal of Petrology*, *28*, 979–1008.

Mahoney, J. J., Saunders, A. D., Storey, M., & Randriamanantenasoa, A. (2008). Geochemistry of the volcan de l'Androy basalt-rhyolite complex, Madagascar Cretaceous igneous province. *Journal of Petrology*, *49*, 1069–1096.

Manhès, G., Allègre, C. J., Dupré, B., & Hamelin, B. (1980). Lead isotope study of basic–ultrabasic layered complexes: Speculations about the age of the earth and primitive mantle characteristics. *Earth and Planetary Science Letters*, *47*, 370–382.

Marsh, B. D. (2002). On bimodal differentiation by solidification front instability in basaltic magmas. Part 1: Basic mechanics. *Geochimica et Cosmochimica Acta*, *66*, 2211–2229.

McClusky, S., Reilinger, R., Ogubazghi, G., Amleson, A., Healeb, B., Vernant, P., Sholan, J., et al. (2010). Kinematics of the southern Red Sea-Afar triple junction and implications for plate dynamics. *Geophysical Research Letters*, *37*, L05301. https://doi.org/10.1029/2009GL041127

Medlin, C. C., Jowitt, S. M., Cas, R. A. F., Howard, H. M., & Wingate, M. T. D. (2014). Petrogenesis of the A-type, Mesoproterozoic intra-caldera rheomorphic Kathleen ignimbrite and comagmatic Rowland suite intrusions, west Musgrave province, central Australia: Products of extreme fractional crystallization in a failed rift setting. *Journal of Petrology*, *56*, 493–525.

Medynski, S., Pik, R., Burnard, P., Dumont, S., Grandin, R., Williams, A., Blard, P.-H., et al., & ASTER team (2016). Magmatic cycles pace tectonic and morphological expression of rifting (Afar depression, Ethiopia). *Earth and Planetary Science Letters*, *446*, 77–88.

Medynski, S., Pik, R., Burnard, P., Vye-Brown, C., France, L., Schimmelpfennig, I., Whaler, K., et al. (2015). Stability of rift axis magma reservoirs: spatial and temporal evolution of magma supply in the Dabbahu rift segment (Afar, Ethiopia) over the past 30 kyr. *Earth and Planetary Science Letters*, *409*, 278–289.

Medynski, S., Pik, R., Burnard, P., Williams, A., Vye-Brown, C., Ferguson, D., Blard, P.-H., et al. (2013). Controls on magmatic cycles and development of rift topography of the Manda Hararo segment (Afar, Ethiopia): Insights from cosmogenic ^{3}He investigation of landscape evolution. *Earth and Planetary Science Letters*, *367*, 133–145.

Melekhova, E., Annen, C., & Blundy, J. (2013). Compositional gaps in igneous rock suites controlled by magma system heat and water content. *Nature Geoscience*, *6*, 385–390.

Miller, J. A., & Harris, C. (2007). Petrogenesis of the Swaziland and northern Natal rhyolites of the Lebombo marginal graben, south east Africa. *Journal of Petrology*, *48*, 185–218.

Natali, C., Beccaluva, L., Bianchini, G., Ellam, R. M., Savo, A., Siena, F., & Stuart, F. M. (2016). High-MgO lavas associated to CFB as indicators of plume related thermochemical effects: The case of ultra-titaniferous picrite–basalt from the Northern Ethiopian–Yemeni Plateau. *Gondwana Research*, *34*, 29–48.

Natali, C., Beccaluva, L., Bianchini, G., & Siena, F. (2011). Rhyolites associated to Ethiopian CFB: Clues for initial rifting at the Afar plume axis. *Earth and Planetary Science Letters*, *312*, 59–68.

Peccerillo, A., Barberio, M. R., Yirgu, G., Ayalew, D., Barberi, M., & Wu, T. W. (2003). Relationships between mafic and acid peralkaline magmatism in continental rift settings: A petrological, geochemical and isotopic study of the Gedemsa volcano, central Ethiopian rift. *Journal of Petrology*, *44*, 2003–2032.

Peccerillo, A., Yirgu, G., & Ayalew, D. (1995). Genesis of acid volcanics along the main Ethiopian rift: A case history of the Gedemsa volcano, SINET: Ethiop. *Journal of Science*, *18*, 23–50.

Pichavant, M., Kontak, D. J., Briqueu, L., Herrera, J. V., & Clark, A. H. (1988). The Miocene-Pliocene Macusani volcanics, SE Peru II. Geochemistry and origin of a felsic peraluminous magma. *Contributions to Mineralogy and Petrology*, *100*, 325–338.

Pik, R., Bellahsen, N., Leroy, S., Denèle, Y., Razin, P., Ahmed, A., & Khanbari, K. (2013). Structural control of basement denudation during rifting revealed by low-temperature (U-Th-Sm)/He thermochronology of the Socotra Island basement-southern Gulf of Aden margin. *Tectonophysics*, *607*, 17–31.

Pik, R., Deniel, C., Coulon, C., Yirgu, G., & Marty, B. (1999). Isotopic and trace element signatures of Ethiopian flood basalts: Evidence for plume-lithosphere interactions. *Geochimica et Cosmochimica Acta*, *63*(15), 2263–2279.

Pik, R., Marty, B., Carignan, J., & Lave, J. (2003). Stability of the upper Nile drainage network (Ethiopia) deduced from (U-Th)/He thermochronometry: Implications for uplift and erosion of the Afar plume dome, Earth Planet. *Science Letters*, *215*, 73–88.

Pik, R., Marty, B., Carignan, J., Yirgu, G., & Ayalew, T. (2008). Timing of east African rift development in southern Ethiopia: Implication for mantle plume activity and evolution of topography. *Geology*, *36*(2), 167–170.

Pin, C., & Zalduegui, J. S. (1997). Sequential separation of light rare-earth elements, thorium and uranium by miniaturized extraction chromatography: Application to isotopic analyses of silicate rocks. *Analytica Chimica Acta*, *339*, 79–89.

Reed, C. A., Almadani, S., Gao, S. S., Elsheikh, A. A., Cherie, S., Abdelsalam, M. G., Thurmond, A. K., et al. (2014). Receiver function constraints on crustal seismic velocities and partial melting beneath the Red Sea rift and adjacent regions, Afar Depression. *Journal of Geophysical Research: Solid Earth*, *119*, 2138–2152. https://doi.org/10.1002/2013JB010719

Reiners, P. W., Nelson, B. K., & Ghiorso, M. S. (1995). Assimilation of felsic crust by basaltic magma: Thermal limits and extents of crustal contamination of mantle-derived magmas. *Geology*, *23*, 563–566.

Riley, T. R., Leat, P. T., Pankhurst, R. J., & Harris, C. (2001). Origins of large volume rhyolitic volcanism in the Antarctic Peninsula and Patagonia by crustal melting. *Journal of Petrology*, *42*, 1043–1065.

Rollinson, H. R. (1993). *Using geochemical data: Evaluation, presentation, interpretation*, *Longman Scientific and Technical* (352 pp.). London: Longman.

Rooney, T. O., Hart, W. K., Hall, C. M., Ayalew, D., Ghiorso, M. S., Hidalgo, P., & Yirgu, G. (2012). Peralkaline magma evolution and the tephra record in the Ethiopian rift. *Contributions to Mineralogy and Petrology*, *164*, 407–426.

Rooney, T. O., Mohr, P., Dosso, L., & Hall, C. (2013). Geochemical evidence of mantle reservoir evolution during progressive rifting along the western Afar margin. *Geochimica et Cosmochimica Acta*, *102*, 65–88.

Selbekk, R. S., & Trønnes, R. G. (2007). The 1362 A.D. Öræfajökull eruption, Iceland: petrology and geochemistry of large-volume homogeneous rhyolite. *Journal of Volcanology and Geothermal Research*, *160*, 42–58.

Stab, M., Bellahsen, N., Pik, R., Quidelleur, X., Ayalew, D., & Leroy, S. (2016). Modes of rifting in magma-rich settings: Tectonic-magmatic evolution of Central Afar. *Tectonics*, *35*, 2–38. https://doi.org/10.1002/2015TC003893

Stern, R. J., & Abdelsalam, M. G. (1998). Formation of juvenile continental crust in the Arabian-Nubian shield: Evidence from granitic rocks of the Nakasib suture, NE Sudan. *Geologische Rundschau*, *87*, 150–160.

Storey, M., Mahoney, J. J., Saunders, A. D., Duncan, R. A., Kelley, S. P., & Coffin, M. F. (1995). Timing of hotspot-related volcanism and the breakup of Madagascar and India. *Science*, *267*, 852–855.

Tanaka, T., Togashi, S., Kamioka, H., & Dragusanu, C. (2000). JNdi-1: A neodymium isotopic reference in consistency with La Jolla neodymium. *Chemical Geology*, *168*, 279–281.

Teklay, M., Kroner, A., & Mezger, K. (2001). Geochemistry, geochronology and isotope geology of Nakfa intrusive rocks, northern Eritrea: products of a tectonically thickened Neoprotezoic arc crust. *Journal of African Earth Sciences*, *33*, 283–301.

Tessema, A., & Antoine, L. A. G. (2004). Processing and interpretation of the gravity field of the east African rift: Implication for crustal extension. *Tectonophysics*, *394*, 87–110.

Thirlwall, M. F. (2002). Multicollector ICP-MS analysis of Pb isotopes using a ^{207}Pb-^{204}Pb double spike demonstrates up to 400 ppm/amu systematic errors in Tl-normalization. *Chemical Geology*, *184*(3), 255–279.

Thorarinsson, S. B., Holm, P. M., Duprat, H. I., & Tegner, C. (2012). Petrology and Sr-Nd-Pb isotope geochemistry of Late Cretaceous continental rift ignimbrites, Kap Washington peninsula, north Greenland. *Journal of Volcanology and Geothermal Research*, *219–220*, 63–86.

Tibari, B., Vacherat, A., Stab, M., Pik, R., Yeghicheyan, D., & Hild, P. (2016). An alternative protocol for single zircon dissolution with application to (U-Th-Sm)/He thermochronometry. *Geostandards and Geoanalytical Research*. https://doi.org/10.1111/j.1751-908X.2016.00375.x

Ukstins, I. A., Renne, P. R., Wolfenden, E. W., Baker, J., Ayalew, D., & Menzies, M. (2002). Matching conjugate volcanic rifted margins: ^{40}Ar/^{39}Ar chrono-stratigraphy of pre- and syn-rift bimodal flood volcanism in Ethiopia and Yemen. *Earth and Planetary Science Letters*, *198*, 289–306.

Varet J. (1975). Carte géologique de l'Afar central et méridional, CNR-CNRS, 1/500 000 Géotechnip.

Vidal, P., Deniel, C., Vellutini, P. J., Coulon, C., Vincent, J., & Audin, J. (1991). Changes of mantle sources in the course of a rift evolution: The Afar case. *Geophysical Research Letters*, *18*, 1913–1916.

White, W. M., Albarède, F., & Tèlouk, P. (2000). High-precision analysis of Pb isotope ratios by multi-collector ICP-MS. *Chemical Geology*, *167*, 257–270.

Woldegabriel, G., Aronson, J. L., & Walter, R. C. (1990). Geology, geochronology, and rift basin development in the central sector of the main Ethiopia rift. *Geological Society of America Bulletin*, *102*, 439–458.

Woldemichael, B. W., Kimura, J.-I., Dunkley, D. J., Tani, K., & Ohira, H. (2010). SHRIMP U-Pb zircon geochronology and Sr-Nd isotopic systematic of the Neoproterozoic Ghimbi-Nedjo mafic to intermediate intrusions of western Ethiopia: A record of passive margin magmatism at 855 Ma. *Geologische Rundschau*, *99*, 1773–1790.

Wolfenden, E., Ebinger, C., Yirgu, G., Renne, P. R., & Kelley, S. P. (2005). Evolution of a volcanic rifted margin: southern Red Sea, Ethiopia. *Geological Society of America Bulletin*, *117*, 846–864.

Wright, T., Ebinger, C., Biggs, J., Ayele, A., Yirgu, G., Keir, D., & Stork, A. (2006). Magma maintained rift segmentation at continental rupture in the 2005 Afar dyking episode. *Nature*, *442*, 291–294.

Zanettin, B., & Piccirillo, E. M. (1980). Correlations among Ethiopian volcanic formations with special references to the chronological and stratigraphic problems of the "Traps Series". *Accademia nazionale dei Lincei Rome*, *47*, 231–252.